*Tools and Resources*

# Multiscale quantification of morphodynamics: MorphoLeaf, software for 2-D shape analysis.

Eric Biot[1,6], Millán Cortizo[1,6], Jasmine Burguet[1,6], Annamaria Kiss[2,3,6], Mohammed Oughou[1], Aude Maugarny-Calès[1,4], Beatriz Gonçalves[1], Bernard Adroher[1], Philippe Andrey[1,5], Arezki Boudaoud[2,3], Patrick Laufs[1]

[1] Institut Jean-Pierre Bourgin, INRA, AgroParisTech, CNRS, Université Paris-Saclay, RD10, 78026 Versailles Cedex, France.

[2] Laboratoire de Reproduction et de Développement des Plantes, INRA, CNRS, ENS de Lyon, UCB Lyon 1, Université de Lyon, 46 Allée d'Italie, 69364 Lyon, Cedex 07, France.

[3] Laboratoire Joliot-Curie, CNRS, ENS de Lyon, Université de Lyon, 46 Allée d'Italie, 69364 Lyon Cedex 07, France.

[4] Univ. Paris-Sud, Orsay, France.

[5] Sorbonne Universités, UPMC Univ Paris 06 UFR 927, Paris, France.

[6] These authors contributed equally to this work.

EB: eric.biot@versailles.inra.fr
MC: mcortizo@gmail.com
JB: Jasmine.Burguet@versailles.inra.fr
AK: annamaria.kiss@ens-lyon.fr
MO: moughou@versailles.inra.fr
AM: aude.maugarny@versailles.inra.fr
BG: Beatriz.Pinto-Goncalves@jic.ac.uk
BA: bernard.adroher@versailles.inra.fr
PA: philippe.andrey@versailles.inra.fr
AB: arezki.boudaoud@ens-lyon.fr
PL: patrick.laufs@versailles.inra.fr

Correspondence should be addressed to J.B. (jasmine.burguet@versailles.inra.fr), A.B. (arezki.boudaoud@ens-lyon.fr) or P.L. (patrick.laufs@versailles.inra.fr).

**Keywords:** multiscale morphometrics, image analysis, leaf, heteroblasty, 2D:4D ratio

**Summary statement:** This paper presents a novel strategy for the analysis and averaging of complex biological 2-D shapes. An application dedicated to the analysis of leaves with different architectures is presented.

**ABSTRACT**

A major challenge in morphometrics is to analyse complex biological shapes formed by structures at different scales. Leaves exemplify this challenge as they combine differences in their overall shape with smaller shape variations at their margin leading to lobes or teeth. Current methods based on contour or on landmarks analysis are successful in quantifying either overall leaf shape or leaf margin dissection, but fail in combining the two. Here, we present a comprehensive strategy and its associated freely available platform for the quantitative, multiscale analysis of the morphology of leaves with different architectures. For this, biologically relevant landmarks are automatically extracted and hierarchized, and used to guide the reconstruction of accurate average contours that properly represent both global and local features. Using this method we established a quantitative framework of the developmental trajectory of Arabidopsis leaves of different ranks and retraced the origin of leaf heteroblasty. When applied to different mutant forms our method can contribute to a better comprehension of gene function as we show here for the role of *CUC2* during Arabidopsis leaf serration. Finally, we illustrated the wider applicability of our tool by analysing hand morphometrics.

## INTRODUCTION

Morphometrics, the quantitative analysis of size and shape of forms, is used to quantify species-to-species variations of complex biological structures, analyze the effects of mutations or environmental factors, describe shape ontogeny or reconstruct the evolution of biological structures in an evo-devo perspective (Adams et al., 2004; Slice, 2007; Klingenberg, 2010).

Leaves are a challenging model for developing novel morphometric methods as they arise in tremendously diverse sizes and shapes (Tsukaya, 2014). The diversity in leaf shape mostly results from variations in their dissection pattern: leaves can be simple when the blade forms a unique unit or compound when it is dissected into multiple leaflets (Blein et al., 2010; Bar and Ori, 2014) (Fig. S1). In addition, the leaf or leaflet margins can be entire, toothed or lobed. Leaf shape is of importance in plants because it contributes to an efficient photosynthesis by affecting not only light interception but also thermoregulation, wind resistance, hydraulic or biomechanical constraints (Nicotra et al., 2011). Accordingly, leaf shape is controlled by both endogenous and environmental factors. As an example, there is a general trend for leaves to be more dissected under colder climates (Royer et al., 2009), which is used to reconstruct the mean annual temperature in paleoclimates (Greenwood, 2005).

Whatever their mature shape, all leaves start their development as small, undissected finger-like primordia that become more complex through differential growth at their margin (Blein et al., 2010). Numerous factors, including transcription factors, miRNAs and hormones controlling leaf development have been identified (Bar and Ori, 2014; Rodriguez et al., 2014; Sluis and Hake, 2015). For instance, transcription factors of the CUP-SHAPED COTYLEDON2 (CUC2) family have a central role in the dissection of the leaf margin into teeth or leaflets (Nikovics et al., 2006; Blein et al., 2008; Berger et al., 2009; Kawamura et al., 2010; Bilsborough et al., 2011; Hasson et al., 2011; Cheng et al., 2012). Other factors have also been shown to affect the patterns of cell division, growth or differentiation and have been associated with changes in leaf shape and/or size (Vlad et al., 2014; Das Gupta and Nath, 2015; Gonzalez et al., 2015). Despite this important progress made in the last years, bridging gene activity with the cellular behaviour and fine changes in leaf shape still remains a challenge, notably because of the difficulty to retrace precisely complex changes in leaf shape throughout their development. More generally, understanding how a primordium develops to reach a complex mature shape would benefit from accurate and precise morphometric analyses.

Different morphometric methods have been deployed for leaves. Discretization of shape based on evenly spaced marks along the contour and averaging these marks over many

leaves allows a proper description and quantification of simple, entire leaves (Langlade et al., 2005; Bensmihen et al., 2008; Weight et al., 2008; Feng et al., 2009). Likewise, landmark-independent Fourier-based analysis of the contour is appropriate to quantify the general shape of the leaf (Chitwood et al., 2012; Chitwood et al., 2013; Chitwood et al., 2014). However, because these approaches result in smooth, averaged contours, none of them is appropriate to accurately capture characteristic structures with a variable position such as teeth or lobes (Chitwood et al., 2012; Chitwood et al., 2013). On the other hand, dissection can be analysed using a few landmarks defined by experts, but the information about the shape between landmarks is lost (Hasson et al., 2011; Viscosi and Cardini, 2011; Klingenberg et al., 2012; Silva et al., 2012; Chitwood et al., 2014; Wang et al., 2014). Global dissection of the leaves can be analysed through the use of the bending energy of the leaf outline (Backhaus et al., 2010; Kuwabara et al., 2011). These examples illustrate the progress made in leaf shape analysis, as well as the difficulties and limitations encountered with morphometric studies in general, underlining the need for a strategy that allows an integrated, multiscale quantification of complex and highly variable shapes.

Here, we present a novel comprehensive method that enables retaining the general shape of objects while preserving proper information for smaller, multiscale structures, together with the MorphoLeaf application that integrates the proposed strategy to analyse and quantify leaf shape. The MorphoLeaf pipeline uses as input a series of leaf images from which landmarks related to its dissection are automatically identified. These landmarks are then used to perform a non-uniform reparametrisation of the leaf outline that enables putting homologous morphological regions over the contour into correspondence. This is the basis for a biologically meaningful computation of mean shapes. The MorphoLeaf application is available as a plug-in for the Free-D software (Andrey and Maurin, 2005). Both the plug-in and the software are freely available. The method can be used to analyse the shape of mature leaves of different architectures or to reconstruct developmentally relevant, meaningful trajectories. As a proof of concept of the usefulness of our method, we reconstructed the developmental trajectory of Arabidopsis leaves of different ranks from their initiation to their mature stage and showed that the heteroblasty observed in mature Arabidopsis leaves results from very early divergent developmental paths. In addition, we performed a fine comparative analysis of early leaf shape between the wild type and the *cuc2* mutant that provides novel insights into the mode of action of *CUC2*, a key regulator of leaf shape (Nikovics et al., 2006; Bilsborough et al., 2011; Hasson et al., 2011). Finally, we showed that MorphoLeaf can have wider application by performing a morphometric analysis of the human hand and in particular

calculating the 2D:4D ratio of the length of second and fourth digits that provides a lifelong signature of prenatal hormonal exposure (Manning et al., 1998; Zheng and Cohn, 2011; Meindl et al., 2012; Sanfilippo et al., 2013)

## RESULTS

We developed the MorphoLeaf application (download from MorphoLeaf.versailles.inra.fr/ user: MorphoLeaf, password: morpho15) to analyse leaf shapes. It involves several steps leading from leaf snapshots to data extraction, quantification, averaging and representation (Fig. 1). At some steps of this pipeline (determination of teeth tip and hierarchy), different alternative methods are proposed; the choice can be made either by visual evaluation of the results or by objectively comparing the results of the proposed methods and of expert analysis on a smaller training set of leaf images. To illustrate the pipeline, we analysed the early stages of leaves 11 to 13 (L11-L13) of short-day grown Arabidopsis plants. These leaves show 3-4 conspicuous teeth on each side of the blade and have a similar course of development (Fig. S2), allowing them to be analysed together as a single data set. Thereby, 207 young leaves ranging from 100 µm to 2500 µm were sampled and imaged under red-chlorophyll fluorescence (Fig. 1A).

### Automated detection of biologically relevant landmarks

*Extraction of the leaf contour*

The leaf outline was automatically extracted using a classical watershed-based method (for a more detailed description as well as for the technical aspects of all methods and algorithms please see the Supplementary Methods) and manually corrected if necessary (~ 30-60 seconds were required per leaf to do the correction, mostly either for young leaves with unclear borders representing ~20% of the leaves in our analysis or for old leaves with deep sinuses representing ~10% of the leaves). During the next step, two landmarks corresponding to the petiole were set manually which allowed the automatic identification of the blade (the side with the greatest area) and the petiole (Fig. 1B). We choose to do this manually (~5 seconds per leaf) as this step is central for further analysis and can not be done automatically for all types of leaves, particularly for young primordia in which the petiole is hardly visible. The leaf tip was then automatically determined as the point of the blade contour furthest away

from the midpoint between petiole landmarks. This also defined the base-tip axis separating the blade in two half blades (Fig. 1C).

*Identification of sinuses and tips of teeth.*

In the next step, we automatically identified the teeth, which are defined as portions of the blade contour comprised between two (not necessarily consecutive, see below) sinuses. Sinuses, which correspond to contour points with a high concave curvature, are identified in a two-step procedure (Fig. SM1 in Supplementary Methods). First, candidate intervals of the contour are determined as connected domains where the curvature remains concave and above a user-defined threshold. Second, within each candidate interval, the point with the maximal curvature is selected as a sinus (Fig. 1C). After automatic detection of sinuses, errors may be manually corrected (~2s per sinus) to ensure that tooth limits are correctly positioned and avoid biases in subsequent analyses (see below for the validation of the automatically detected sinuses).

After sinus identification, MorphoLeaf determines the position of the tooth tip between consecutive sinuses (Fig. 1C). The user can choose one of the two strategies available depending on tooth shapes. For rather sharp teeth, the selected tip corresponds to the point with a maximal local curvature. For round teeth like those in young Arabidopsis leaves, we developed an alternative strategy based on the observation that towards its tip, the tooth is rather symmetrical (Fig. SM2 in Supplementary Methods). Hence, the tooth tip is defined as the contour point that maximizes a local symmetry criterion.

*Teeth hierarchy determination*

Using the methods described above, we could identify the teeth along the leaf blade. However, a close examination of leaves of Arabidopsis (Fig. 1C,D and Fig. SM3 in Supplementary Methods) and of other species (Fig. S3) showed that teeth sometimes have a hierarchical organisation: a primary tooth is any tooth that developed on the main leaf contour, whereas a secondary tooth is formed on a primary tooth. It is essential to take this tooth hierarchy into account for further analyses as for instance the area of a primary tooth includes the areas of all higher order teeth that it carries.

To determine teeth hierarchy, the user can choose between two methods, each adapted to leaves with different architectures.

The first method is iterative and based on the observation that, in contrary to the secondary sinuses, the primary sinuses are well positioned on the basal leaf contour (i.e., a

smooth contour in which teeth have been erased) (Fig. SM4 in Supplementary Methods). Based on this criterion, at each iteration, a candidate secondary sinus (i.e., with a degree of misalignment with the basal contour above a detection threshold) is identified and removed from the set of primary sinuses. The process is repeated until no additional sinus can be recognised as a secondary sinus (i.e., the misalignment degrees of remaining sinuses are all below the detection threshold).

The second method is a recursive algorithm adapted to developing leaves that relies upon the assumption that the tooth inclination increases with the rank (Fig. SM5 in Supplementary Methods). The orientation threshold that determines if a higher hierarchy is detected is the sole parameter of the algorithm. This method is adapted to leaves like the ones in Arabidopsis in which the basal leaf contour tends to exhibit a rather regular (convex) curvature. Using this method eight secondary teeth were detected in our Arabidopsis set of images.

The outcome of the two methods can be represented by a hierarchical tree in which a node corresponds to a single tooth, whose rank is given by its level in the tree. In addition, sinuses are labelled with a "primary" or "secondary" tag. The term "secondary" generalizes to all teeth with a rank strictly superior to 1 because it is sufficient to identify primary teeth and their associated, higher rank structures.

*Validation of automatic sinus detection and hierarchy*

In order to quantify the performance of our semi-automatic sinus detection, we compared its results with manual marking performed independently by four experts on a test data set of leaf images (Figs. SM7 and SM8 in Supplementary Methods). For this, we implemented an algorithm that matches landmarks corresponding to the same biological features both in expert and algorithm results (Fig. SM6 in Supplementary Methods). Then, we compared the distances between automatically detected sinuses and those detected by experts and we showed that several combinations of parameters provided an automatic sinus positioning within the limits of the inter-expert variability (e.g., ~1-3 µm for Arabidopsis leaves from 500 to 2000 µm, Fig. SM7 in Supplementary Methods). Similarly, several combinations of parameters generated numbers of false positive and of false negative detections within the range of those generated by the experts. Altogether, this indicates a good performance of our method in term of success rate and precision. Similarly, we evaluated the two methods of hierarchy detection, both showing highly satisfactory sensibility and specificity (Tables 1 and 2 in Supplementary Methods).

**Landmark-based quantification of the shape of Arabidopsis leaves L11, L12 and L13**

Using the automatically detected landmarks, we quantified different parameters associated with either the entire leaf or individual teeth. We plotted measurements against blade length which is used here as a proxy for the stage of development. Blade growth is globally isotropic as the ratio between blade width and length remains constant, while area increases quadratically (Fig. 2A,B). Teeth appear sequentially along the leaf margin and tend to be synchronous on both sides of the leaf, since leaves with even teeth numbers were more frequent than leaves with odd numbers (Fig. 2C). There was however an important variability of the leaf size at which teeth initiated. For instance, the first pair of teeth is formed when the blade is between 110 and 333 µm long. The dynamics of individual tooth development was reconstructed and showed that teeth later arising are more pointy than the first ones (Fig. 2D-G). The evolution of the relative position of the sinuses along the proximodistal leaf axis revealed heterogeneous growth of the blade along this axis, with a more important relative growth in the region where the first pair of teeth develops (Fig. 2H,I).

**Reconstruction of teeth and whole leaves developmental trajectories**

*Developmental trajectories of teeth*

To analyse tooth shape, we next extracted contours corresponding to teeth 1, 2 and 3, *i.e.* the part of the blade outline situated between two consecutive primary sinuses. In order to put size effects aside, we rescaled all primary teeth by registering their two sinuses. Then, we performed a principal component analysis (PCA) to analyse variations in tooth shape (Fig. 3A,B) as previously described for the whole leaf contours (Langlade et al., 2005; Bensmihen et al., 2008; Feng et al., 2009; Chitwood et al., 2014). The first axis corresponds to the variation in tooth height and confirms the difference in pointedness observed between tooth 1 and teeth 2 and 3. Interestingly, variation along the second axis, which corresponds to the degree of tooth asymmetry, showed that there is an increasing asymmetry from tooth 1 to tooth 3.

*Developmental trajectories of the whole leaf*

Although very informative, the analyses performed above do not place the teeth in the context of the whole leaf. Therefore, we included in MorphoLeaf methods to construct mean shapes and to integrate mean contours in the context of the growth dynamics. In order to build mean growth trajectories, we proposed two strategies. In the first one, leaves are ordered by blade length and then sorted into length classes (bins) before averaging in each bin. Instead of

fixing bins, the second strategy is based on a moving average approach using an adaptive kernel method in which the user can control the range of leaves that contribute to the averaging with a bandwidth parameter (see Supplementary Methods).

The basic strategy to produce an average leaf shape is to define $N$ points regularly distributed over the contour of different leaf samples, and take the average of every $n$-th point ($1 \leq n \leq N$) to compute an average leaf contour (Langlade et al., 2005; Bensmihen et al., 2008; Feng et al., 2009; Chitwood et al., 2014). However, because the number and position of the teeth along the margin vary between different samples, the $n$-th point may not correspond to the same biological feature in different samples (Fig. 3C, left panel). This strategy generally yields a smoothed contour with partially erased teeth. Overcoming this problem is a key contribution of our work. We took advantage of our automatic landmark-detection and classification algorithm, which identifies an important set of homologous landmarks on the contours, and we introduced a reparametrisation of the contour so that homologous landmarks as well as homologous contour regions in between these landmarks are always in correspondence (Fig 3C, right panel). Finally, the contour between homologous landmarks in different leaves is discretized with the same number of points.

We tested the effects of increasing the number of landmarks to guide the reparametrisation by sequentially adding: i) the leaf tip, ii) teeth sinuses and iii) teeth tips (Fig. 3D) and evaluated the accuracy of the generated mean shapes (Fig. 3E,F) by comparing their morphological parameters with those directly extracted from the individual leaves that were used to generate mean shapes (Fig 3G-I). The overall leaf shape was mostly insensitive to the number of landmarks used to guide the reparametrisation, and both instances produced accurate leaf areas (Fig. 3G). However, adding landmarks significantly improved the quality of the teeth contours around the landmarks included and also along the whole leaf contour (Fig. 3D). Quantification of tooth height and area confirmed the visual observation that increasing the number of landmarks in the reparametrisation increases the accuracy of the mean teeth shapes (Fig. 3D,H,I).

In conclusion, using all landmarks to guide the contour reparametrisation, we could assess an accurate developmental trajectory of Arabidopsis young leaves L11 to L13.

**Reconstruction of mature leaf shape in different species**

MorphoLeaf was successfully applied to describe and quantify the shape of Arabidopsis leaves. To see how MorphoLeaf performs in a broader context, we tested it on various plant species (Fig. 4, Fig. S4 and Table S1). For all considered species, the maximal curvature and

the iterative method were well suited to determine teeth tips and hierarchy, respectively. Reparametrisation based on landmarks appeared also essential to obtain representative contours for the mean leaves. Thus, MorphoLeaf can be effectively used to analyse the shapes and to reconstruct the mean contours of mature leaves with different architectures such as pinnately and palmately lobed leaves, pinnately lobed with secondary structures and palmately compound leaves (Fig. 4). Current limitations of the MorphoLeaf application include the hierachisation of several levels of dissection in palmately lobed leaves, an accurate quantification of pinnately compound leaves and the analysis of samples with a strong heterogeneity in structure sizes and numbers (Fig. S5).

**Reconstruction of the developmental trajectory of Arabidopsis leaves of different ranks.**

Leaves successively formed during a plant's life often differ in their mature shapes, a phenomenon described as leaf heteroblasty (Poethig, 1997; Tsukaya et al., 2000; Zotz et al., 2011). Using MorphoLeaf, we reconstructed and quantified mean mature leaves L01, L03, L05, L07, L09 and L11 from short-day-grown Arabidopsis to quantify the heteroblasty level (Fig. 5A and Fig. S6). This showed that vegetative leaves of increasing rank become more elongated with more and bigger teeth.

Next we reconstructed the developmental trajectory of leaves of different ranks. For this we collected individual leaves from their initiation to their mature stage (between 160 and 312 leaves per rank, average 196) and analysed them using MorphoLeaf. The evolution of the shape of leaves of different ranks could be reconstructed (Fig. 5B-I, Fig. S7 and Movies 1-12) and in parallel leaf morphological parameters quantified (Fig. 5J-O). Careful observation of mean leaf shapes (*e.g.* L01 in Fig. 5H,I and Fig. S7) and the analysis of the number of teeth along the development (Fig. 5K) revealed a feature common to all leaf ranks: after an initial increase in the number of teeth, reflecting their successive initiation, the number of teeth decreases. This apparent "disappearance" of teeth is due to a progressive smoothening of the sinus of the most distal teeth (Fig. S7). As a consequence, the homology between teeth is lost: a tooth 2 becomes a tooth 1 when the most distal tooth 1 disappears. To keep the homology between teeth throughout leaf development, we re-examined the most mature leaves and manually added distal teeth if required in order to follow the dynamics of teeth formation before generating the data describing teeth morphometrics (Fig 5L-O).

**Developmental origin of leaf heteroblasty.**

We next investigated the developmental trajectory leading to leaf heteroblasty in Arabidopsis. Two extreme mechanisms can be envisaged: primordia of leaves of different ranks may be different from their early stages onwards or, alternatively, they could be similar during early phases of development and diverge during later phases. To answer this question we used MorphoLeaf to compare the evolution of the shape of leaves from different ranks and the associated quantitative parameters (Fig. 5F-O).

Shortly after initiation (at 200 µm-long), leaf primordia showed a similar shape, though later on leaves of lower rank become wider than higher rank leaves (Fig. 5F-J). More teeth are initiated on smaller primordia of higher rank leaves (Fig. 5F-I,K) and on a more distal position along the primordium (Fig. 5G,H,L). This indicates that primordia of different ranks already show divergent features soon after their initiation.

While the increase in teeth width is similar in all leaves (except L01, Fig. 5M), increase in height is more important in higher rank leaves (Fig. 5N). However, the evolution of the relative teeth area indicates that the dynamics of teeth growth is similar for all leaves, except L01 (Fig. 5O). Together, this shows that teeth are more pointed in higher rank leaves due to a faster increase in height.

Altogether, this analysis shows that heteroblasty in Arabidopsis results from divergence in developmental trajectories from the very early stages of leaf formation. These differences are enhanced during later steps of teeth growth. Although the patterning of the margin is mostly established during the initial phases of leaf development, it is rearranged during later stages as shown by the smoothening of the most distal dissections.

**Role of *CUC2* during leaf serration.**

*CUC2* is an important regulator of leaf margin serration and has been proposed to either locally repress growth to form the teeth sinuses (Nikovics et al., 2006) to promote teeth outgrowth (Kawamura et al., 2010) or a combination of both (Bilsborough et al., 2011). We used MorphoLeaf to finely compare early stages of leaf development between the wild type and the *cuc2-1* mutant (Fig. 6). At 175 µm-long, while the *cuc2-1* mutant leaf primordium has a smooth, convex outline, two faint creases have formed in the wild type, at the sites where a *CUC2:CUC2:VENUS* translational reporter is expressed (Fig. 6A-B). This shows that the first visible effect of CUC2 activity is a local repression of growth. This effect is maintained during later stages (Fig. 6C-F). In primordia above 225 µm-long, teeth outgrowth becomes visible in the wild type compared to the *cuc2-1* mutant, indicating that during a

second phase, teeth formation is associated with a local increase in growth, which may result from an increased cell proliferation and/or expansion. Together, these observations suggest a dual role for *CUC2* during leaf serration.

**Applying MorphoLeaf to analyse hand morphometrics**

To test the robustness of MorphoLeaf, we experimented its applicability to other 2-D structures. Hand morphometrics relies on the analysis of a 2-D structure with protruding outgrowths (the fingers). In particular the 2D:4D ratio of the length of second and fourth digits provides a signature of the prenatal hormonal exposure and has been associated with several adult characteristics including behaviour, fertility and disease risk (McIntyre, 2006). MorphoLeaf allowed the automatic identification of 10 of the 12 landmarks necessary to measure the length of all fingers (Fig. 7A-C). Using landmark-guided reparametrisation we could reconstitute average hand shapes (Fig. 7D-E) in which finger length was properly represented (Fig. 7G-H) and calculate the widely used 2D:4D ratio. This shows that MorphoLeaf can be widely used to analyse complex 2-D biological objects.

## DISCUSSION

Morphometrics is usually based on either the analysis of the outline of the biological object or on biological landmarks (Adams et al., 2004; Slice, 2007; Klingenberg, 2010). Here, we propose a new method that combines both approaches. Biologically relevant landmarks are automatically identified and used to reparametrise the outline, which allows putting homologous points in correspondence before averaging the outline of several objects. This reparametrisation is essential to obtain average shapes that are representative of individual leaves. Adding as few as one landmark (the leaf apex) substantially increases the quality of the averaging. Automation of the landmark detection contributes to the reproducibility of the results by limiting variations due to placement by operators. Using this new approach we provide quantifications (number, size, shape, and position) of multiple structures present in the object and a faithful representation of the mean shape of the object. These two outcomes are complementary as the quantifications allow for the analysis of precise features on any structure of the object associated with the landmarks, while the mean shape allows to better capture the complexity of the biological object as a whole (including regions not directly associated with a particular landmark). The mean representation is also extremely helpful to follow developmental trajectories. The reparameterised outline can also be analysed by Principal Component Analysis (PCA, Fig. S8). It should be noted that because the coordinates of the landmarks are recorded, geometric morphometric methods such as Generalized Procrustes Analysis (GPA) can also be applied to the data provided by MorphoLeaf.

Using MorphoLeaf we generated the developmental sequence of Arabidopsis leaves of different ranks. We show that the acquisition of mature leaf shape is a complex process that takes place early on when the teeth are initiated along the leaf margin but that is refined during later stages. Indeed, teeth successively initiated along the leaf margin show different growth dynamics resulting in different shapes (Fig 2E,F). In addition, the most distal teeth are eroded during the later stages and are no more detectable in the mature leaves. This underlines the importance of reconstructing the entire developmental sequence to fully understand the ontology processes leading to mature leaf shapes. More generally, any molecular or cellular data collected during the course of leaf development could be mapped on the morphological framework generated here, which is a first step towards the production of a virtual leaf. In addition, our method provides information on the distribution of growth within the leaf. For instance, the evolution of the ratio between the area of a tooth and that of the whole leaf provides insight into the dynamics of tooth growth. The evolution of the relative position of

the teeth sinuses along the leaf proximo-distal axis provides quantitative information about the growth gradient along this axis. Indeed, our observations of leaves > 2mm in length (Fig. S9) are in agreement with a growth arrest front starting at the leaf tip and progressing proximally (Remmler and Rolland-Lagan, 2012) while the data retrieved from earlier stages show that growth is enhanced in the central part of the primordium (Fig. 2H,I). This was not observed in the first leaves (Kuchen et al., 2012).

By comparing the developmental sequences of leaves of different ranks we showed that leaf heteroblasty results from differences in early pattern of teeth initiation (position along the leaf primordium and size of the primordium at teeth initiation) and differential outgrowth of the teeth. This analysis also underlines the complementarity between the two types of data produced by MorphoLeaf, the average mean shapes and the quantification of biological structures.

The precise morphological data on teeth development generated by MorphoLeaf helps determining how the activity of members of previously identified genetic and molecular networks precisely affect leaf morphogenesis, as illustrated here for *CUC2*. *CUC2* has been suggested to lead to Arabidopsis leaf serration by two mechanisms: repression of growth to form the sinuses and/or growth promotion to lead to teeth outgrowth (Nikovics et al., 2006; Kawamura et al., 2010; Bilsborough et al., 2011). Our precise comparison of the early shapes of wild type *versus cuc2* mutants indeed showed that the two mechanisms occur but at different stages. The first detectable effect of *CUC2* activity is a local repression of growth while only slightly later an outgrowth becomes observable at distance from the *CUC2* expression domain. This indicates that *CUC2* may shape the margin of simple leaves by a dual mechanisms similar to the one proposed for other *NAM*/*CUC3* genes during compound leaf development (Blein et al., 2008). Several different scenarios could be put forward to explain this observed sequence of morphological changes. *CUC2* expression could repress growth locally while simultaneously producing a signal that could promote growth at distance, the delay between the observation between these two processes resulting from the time necessary for the signal to be produced, migrate through part of the leaf and be transduced in a detectable change in shape. For instance the generation of CUC2-dependant auxin activity maxima could be such a signal (Bilsborough et al., 2011). Alternatively, changes in the growth pattern at sinuses could indirectly modify growth at distance. Identification of the network acting downstream of CUC2 could possibly help discriminating between these scenarios.

To illustrate the genericity of our approach we analysed the morphology of simple leaves with different architectures. In the case of complex morphologies, the identification of the observed hierarchical structure is central to an accurate shape analysis as it allows selecting the homologous landmarks used for the landmark-guided reparametrisation. Our method could be also directly applied to hand-selected individual leaflets. A similar strategy could be used to improve the analysis of any object by providing an accurate description of the outline between different landmarks. Finally, we showed that MorphoLeaf can be applied to other morphometric studies like for instance morphometrics of human hands and the calculation of the 2D:4D ratio. Therefore, the MorphoLeaf application provides not only a valuable tool to quantify and represent truthfully complex leaf shapes, but the strategy described here could also be used for morphometric studies of other models.

## MATERIALS AND METHODS

### Plant material and growth conditions

All Arabidopsis plants are in the Columbia-0 background. The *cuc2-1* mutant and *CUC2-CUC2-VENUS* reporter line have been described elsewhere (Hasson et al., 2011; Goncalves et al., 2015). The *mir164a-4* mutant (Nikovics et al., 2006) that shows a higher level of leaf was used to validate the hierarchy procedure. Seeds were stratified for 2 days, in water, at 4°C in the dark prior to sowing. Plants were grown on soil in short-day conditions [1 hour dawn (19°C, 65% hygrometry, 80 µMol/m²/s light), 6 hours day (21°C, 65% hygrometry, 120 µMol/m²/s light), 1 dusk (20°C, 65% hygrometry, 80 µMol/m²/s light), 16 hours dark (18°C, 65% hygrometry, no light)]. The short-day conditions allowed us to have plants that stay longer in the vegetative phase and to obtain more leaves per plant.

Mature leaves from other species were collected in the park surrounding the INRA center in Versailles and identified using different flora determination books or were extracted from the Middle European Woods data base (Novotný and Suk, 2013).

### Leaf dissection and imaging

Leaves number L01, L03, L05, L07, L09, L11, L12 and L13 were dissected using a medical needle, mounted on a slide and imaged with a binocular on chlorophyll fluorescence at early stages and white light at later stages. Mounting media has the following composition: Tris HCl 10mM pH=8,5, Triton 0.01%. Mature leaves of Arabidopsis and other species were scanned at a resolution ranging from 1200 to 1600 dpi depending on the leaf complexity.

The MorphoLeaf application can be downloaded from **MorphoLeaf.versailles.inra.fr/**

The methods of the MorphoLeaf application are described in detail in the Supplementary Methods.

**Acknowledgements**

We thank C. Godin for very fruitful discussions during this work, V. Mirabet for suggestions, T. Blein and N. Arnaud for comments on the manuscript and Joris Martinez for his help in the study of the *cuc2-1* mutant. We thank members of the IJPB lab who "gave a hand" to this project.

**Competing interests**

The authors declare no competing or financial interests.

**Author contributions**

EB, MC, JB, AK, MO, AB and PL conceived the MorphoLeaf application that was encoded by EB with the help of PA. MC, AM, BG, BA and PL performed the experiments and EB, MC JB, AK, AB and PL analysed the data. JB, EB and PL wrote the paper with input from all other authors.

**Funding**

This work was supported by the Agence National de la Recherche grants MorphoLeaf (project reference ANR-10-BLAN-1614) and LeafNet (project reference ANR-12-PDOC-0003). MC was partly supported by the Fundacion Alfonso Martin Escudero. The IJPB benefits from the support of the Labex Saclay Plant Sciences-SPS (ANR-10-LABX-0040-SPS).

## REFERENCES


**Adams, D. C., Rohlf, F. J. and Slice, D. E.** (2004) Geometric morphometrics: Ten years of progress following the 'revolution'. *Ital. J. Zool* **71**, 5-16.

**Andrey, P. and Maurin, Y.** (2005) Free-D: an integrated environment for three-dimensional reconstruction from serial sections. *J Neurosci Methods* **145**, 233-244.

**Backhaus, A., Kuwabara, A., Bauch, M., Monk, N., Sanguinetti, G. and Fleming, A.** (2010) LEAFPROCESSOR: a new leaf phenotyping tool using contour bending energy and shape cluster analysis. *New Phytol* **187**, 251-261.

**Bar, M. and Ori, N.** (2014) Leaf development and morphogenesis. *Development* **141**, 4219-4230.

**Bensmihen, S., Hanna, A. I., Langlade, N. B., Micol, J. L., Bangham, A. and Coen, E. S.** (2008) Mutational spaces for leaf shape and size. *HFSP J* **2**, 110-120.

**Berger, Y., Harpaz-Saad, S., Brand, A., Melnik, H., Sirding, N., Alvarez, J. P., Zinder, M., Samach, A., Eshed, Y. and Ori, N.** (2009) The NAC-domain transcription factor GOBLET specifies leaflet boundaries in compound tomato leaves. *Development* **136**, 823-832.

**Bilsborough, G. D., Runions, A., Barkoulas, M., Jenkins, H. W., Hasson, A., Galinha, C., Laufs, P., Hay, A., Prusinkiewicz, P. and Tsiantis, M.** (2011) Model for the regulation of Arabidopsis thaliana leaf margin development. *Proc Natl Acad Sci U S A* **108**, 3424-3429.

**Blein, T., Hasson, A. and Laufs, P.** (2010) Leaf development: what it needs to be complex. *Curr Opin Plant Biol* **13**, 75-82.

**Blein, T., Pulido, A., Vialette-Guiraud, A., Nikovics, K., Morin, H., Hay, A., Johansen, I. E., Tsiantis, M. and Laufs, P.** (2008) A conserved molecular framework for compound leaf development. *Science* **322**, 1835-1839.

**Cheng, X., Peng, J., Ma, J., Tang, Y., Chen, R., Mysore, K. S. and Wen, J.** (2012) NO APICAL MERISTEM (MtNAM) regulates floral organ identity and lateral organ separation in Medicago truncatula. *New Phytol* **195**, 71-84.

**Chitwood, D. H., Headland, L. R., Kumar, R., Peng, J., Maloof, J. N. and Sinha, N. R.** (2012) The developmental trajectory of leaflet morphology in wild tomato species. *Plant Physiol* **158**, 1230-1240.

**Chitwood, D. H., Kumar, R., Headland, L. R., Ranjan, A., Covington, M. F., Ichihashi, Y., Fulop, D., Jimenez-Gomez, J. M., Peng, J., Maloof, J. N. et al.** (2013) A quantitative genetic basis for leaf morphology in a set of precisely defined tomato introgression lines. *Plant Cell* **25**, 2465-2481.

**Chitwood, D. H., Ranjan, A., Martinez, C. C., Headland, L. R., Thiem, T., Kumar, R., Covington, M. F., Hatcher, T., Naylor, D. T., Zimmerman, S. et al.** (2014) A modern ampelography: a genetic basis for leaf shape and venation patterning in grape. *Plant Physiol* **164**, 259-272.

**Das Gupta, M. and Nath, U.** (2015) Divergence in Patterns of Leaf Growth Polarity Is Associated with the Expression Divergence of miR396. *Plant Cell* **27**, 2785-2799.

**Feng, X., Wilson, Y., Bowers, J., Kennaway, R., Bangham, A., Hannah, A., Coen, E. and Hudson, A.** (2009) Evolution of allometry in antirrhinum. *Plant Cell* **21**, 2999-3007.

**Goncalves, B., Hasson, A., Belcram, K., Cortizo, M., Morin, H., Nikovics, K., Vialette-Guiraud, A., Takeda, S., Aida, M., Laufs, P. et al.** (2015) A conserved role for CUP-SHAPED COTYLEDON genes during ovule development. *Plant J* **83**, 732-742.

**Gonzalez, N., Pauwels, L., Baekelandt, A., De Milde, L., Van Leene, J., Besbrugge, N., Heyndrickx, K. S., Perez, A. C., Durand, A. N., De Clercq, R. et al.** (2015) A Repressor Protein Complex Regulates Leaf Growth in Arabidopsis. *Plant Cell* **27**, 2273-2287.
**Greenwood, D. R.** (2005) Leaf form and the reconstruction of past climates. *New Phytol* **166**, 355-357.
**Hasson, A., Plessis, A., Blein, T., Adroher, B., Grigg, S., Tsiantis, M., Boudaoud, A., Damerval, C. and Laufs, P.** (2011) Evolution and Diverse Roles of the CUP-SHAPED COTYLEDON Genes in Arabidopsis Leaf Development. *Plant Cell* **23**, 54-68.
**Kawamura, E., Horiguchi, G. and Tsukaya, H.** (2010) Mechanisms of leaf tooth formation in Arabidopsis. *Plant J* **62**, 429-441.
**Klingenberg, C. P.** (2010) Evolution and development of shape: integrating quantitative approaches. *Nat Rev Genet* **11**, 623-635.
**Klingenberg, C. P., Duttke, S., Whelan, S. and Kim, M.** (2012) Developmental plasticity, morphological variation and evolvability: a multilevel analysis of morphometric integration in the shape of compound leaves. *J Evol Biol* **25**, 115-129.
**Kuchen, E. E., Fox, S., de Reuille, P. B., Kennaway, R., Bensmihen, S., Avondo, J., Calder, G. M., Southam, P., Robinson, S., Bangham, A. et al.** (2012) Generation of leaf shape through early patterns of growth and tissue polarity. *Science* **335**, 1092-1096.
**Kuwabara, A., Backhaus, A., Malinowski, R., Bauch, M., Hunt, L., Nagata, T., Monk, N., Sanguinetti, G. and Fleming, A.** (2011) A shift towards smaller cell size via manipulation of cell cycle gene expression acts to smoothen Arabidopsis leaf shape. *Plant Physiol*.
**Langlade, N. B., Feng, X., Dransfield, T., Copsey, L., Hanna, A. I., Thebaud, C., Bangham, A., Hudson, A. and Coen, E.** (2005) Evolution through genetically controlled allometry space. *Proc Natl Acad Sci U S A* **102**, 10221-10226.
**Manning, J. T., Scutt, D., Wilson, J. and Lewis-Jones, D. I.** (1998) The ratio of 2nd to 4th digit length: a predictor of sperm numbers and concentrations of testosterone, luteinizing hormone and oestrogen. *Hum Reprod* **13**, 3000-3004.
**McIntyre, M. H.** (2006) The use of digit ratios as markers for perinatal androgen action. *Reprod Biol Endocrinol* **4**, 10.
**Meindl, K., Windhager, S., Wallner, B. and Schaefer, K.** (2012) Second-to-fourth digit ratio and facial shape in boys: the lower the digit ratio, the more robust the face. *Proc Biol Sci* **279**, 2457-2463.
**Nicotra, A. B., Leigh, A., Boyce, C. K., Jones, C. S., Niklas, K. J., Royer, D. L. and Tsukaya, H.** (2011) The evolution and functional signi!cance of leaf shape in the angiosperms. *Funct Plant Biol* **38**, 535-552.
**Nikovics, K., Blein, T., Peaucelle, A., Ishida, T., Morin, H., Aida, M. and Laufs, P.** (2006) The balance between the MIR164A and CUC2 genes controls leaf margin serration in Arabidopsis. *Plant Cell* **18**, 2929-2945.
**Novotný, P. and Suk, T. (2013)** Leaf recognition of woody species in Central Europe. *Biosys. Eng.* **115**, 444-452.
**Poethig, R. S.** (1997) Leaf morphogenesis in flowering plants. *Plant Cell* **9**, 1077-1087.
**Remmler, L. and Rolland-Lagan, A. G.** (2012) Computational method for quantifying growth patterns at the adaxial leaf surface in three dimensions. *Plant Physiol*.
**Rodriguez, R. E., Debernardi, J. M. and Palatnik, J. F.** (2014) Morphogenesis of simple leaves: regulation of leaf size and shape. *Wiley Interdiscip Rev Dev Biol* **3**, 41-57.
**Royer, D. L., Meyerson, L. A., Robertson, K. M. and Adams, J. M.** (2009) Phenotypic plasticity of leaf shape along a temperature gradient in Acer rubrum. *PLoS One* **4**, e7653.

**Sanfilippo, P. G., Hewitt, A. W., Mountain, J. A. and Mackey, D. A.** (2013) A geometric morphometric assessment of hand shape and comparison to the 2D:4D digit ratio as a marker of sexual dimorphism. *Twin Res Hum Genet* **16**, 590-600.
**Silva, M. F. S., De Andrade, I. M. and Mayo, S. J.** (2012) Geometric morphometrics of leaf blade shape in Montrichardia linifera (Araceae) populations from the Rio Parnaíba Delta, north-east Brazil. . *Bot. J. Linnean Soc.* **170**, 554-572.
**Slice, D. E.** (2007) Geometric Morphometrics. *Annu. Rev. Anthropol.* **36**, 261-281.
**Sluis, A. and Hake, S.** (2015) Organogenesis in plants: initiation and elaboration of leaves. *Trends Genet* **31**, 300-306.
**Tsukaya, H.** (2014) Comparative leaf development in angiosperms. *Curr Opin Plant Biol* **17**, 103-109.
**Tsukaya, H., Shoda, K., Kim, G. T. and Uchimiya, H.** (2000) Heteroblasty in Arabidopsis thaliana (L.) Heynh. *Planta* **210**, 536-542.
**Viscosi, V. and Cardini, A.** (2011) Leaf morphology, taxonomy and geometric morphometrics: a simplified protocol for beginners. *PLoS One* **6**, e25630.
**Vlad, D., Kierzkowski, D., Rast, M. I., Vuolo, F., Dello Ioio, R., Galinha, C., Gan, X., Hajheidari, M., Hay, A., Smith, R. S. et al.** (2014) Leaf shape evolution through duplication, regulatory diversification, and loss of a homeobox gene. *Science* **343**, 780-783.
**Wang, X. M., Hou, X. Q., Zhang, Y. Q. and Li, Y.** (2014) Morphological variation in leaf dissection of Rheum palmatum complex (Polygonaceae). *PLoS One* **9**, e110760.
**Weight, C., Parnham, D. and Waites, R.** (2008) LeafAnalyser: a computational method for rapid and large-scale analyses of leaf shape variation. *Plant J* **53**, 578-586.
**Zheng, Z. and Cohn, M. J.** (2011) Developmental basis of sexually dimorphic digit ratios. *Proc Natl Acad Sci U S A* **108**, 16289-16294.
**Zotz, G., Wilhelm, K. and Becker, A.** (2011) Heteroblasty A review. *Bot. Rev.* **77**, 109-151.

**Figures**

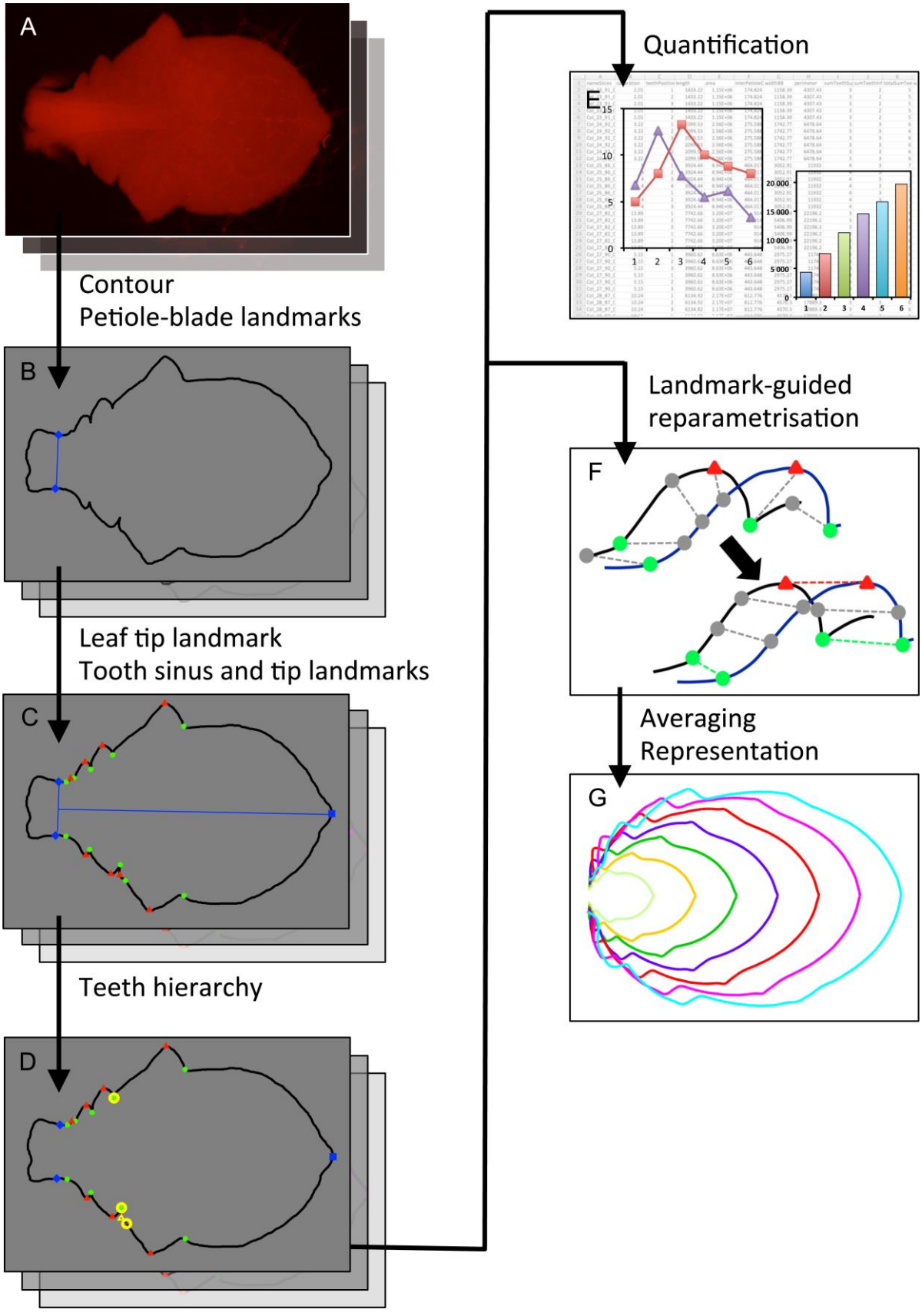

**Figure 1. Overview of the MorphoLeaf tool**. The MorphoLeaf tool is an application that runs on the freely available Free-D software. (**A**) The input data are stacks of leaf pictures. (**B**) The leaves are automatically segmented to extract the leaf contour. The user sets two landmarks on the leaf contour at the junction between the petiole and the blade (blue diamonds). (**C**) The tip of the leaf (blue square), the sinuses of the teeth (green dots) and the tips of the teeth (red triangles) are automatically positioned. (**D**) If required, the hierarchical structure of the teeth can be automatically determined to identify primary teeth and higher ordered structures that are formed on them (secondary tooth sinuses indicated by yellow circles and secondary tooth tips indicated by yellow triangles). The multiple leaf contours bearing biologically relevant landmarks of a stack can be analysed in two ways. (**E**) First, quantitative data for the biologically relevant features characterising the leaf structure (*e.g.* size of the leaf or the teeth, position of the teeth along the leaf) can be automatically extracted for each leaf of the stack. (**F**,**G**) Second, mean shapes can be generated. For this, a nonlinear landmark-guided reparametrisation of the leaf contour is performed to put homologous point of the contour into correspondence before mean shapes are computed (**F**). The reparametrised contours are then used to generate mean contours either from all pictures of the stack or from multiple selections of pictures (**G**).

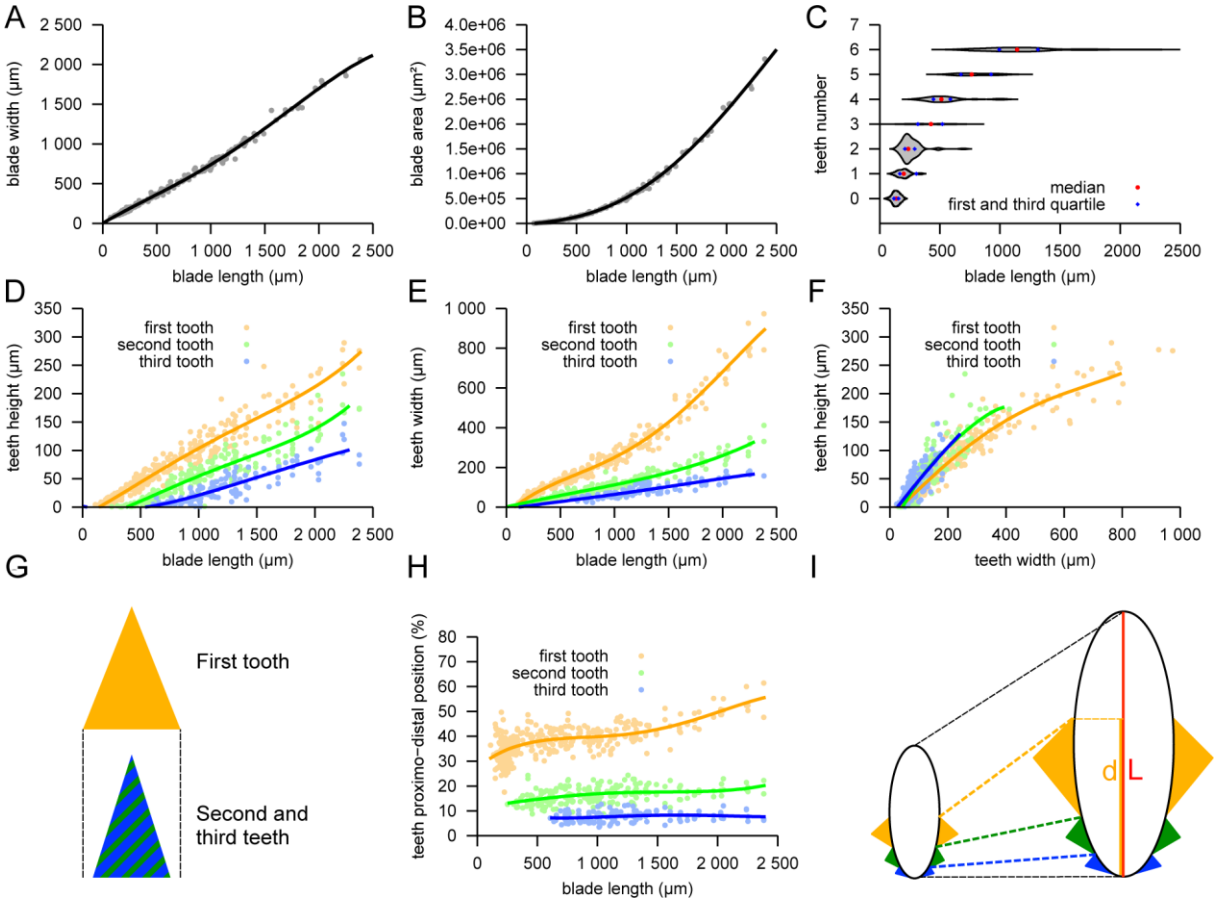


**Figure 2. Morphometrics of young leaves L11-L13 based on biologically relevant landmarks extracted using MorphoLeaf**.

Morphological parameters were extracted for young L11-L13 leaves based on biologically relevant landmarks determined by MorphoLeaf. Quantifications were performed on the whole leaf (**A-C**) or on tooth 1, 2, or 3 (**D-H**, teeth numbered according to their position on each side of the leaf blade starting from the tip to the base, which also corresponds to their order of initiation). Blade width (**A**), blade area (**B**) and teeth number (**C**) plotted against blade length. Tooth height (**D**) and tooth width (**E**) plotted against blade length. Tooth height plotted against tooth width (**F**) and scheme showing the difference in shape between tooth 1 and teeth 2 and 3 deduced from panel F (**G**). Relative proximo-distal position of the distal sinus of teeth 1 to 3 (measured as the ratio of the distance of the projected distal sinus on the leaf axis to the base of the leaf blade (d in **I**) divided by the blade length (L in **I**)) plotted against blade length (**H**). Scheme of the evolution of the position of the tooth sinuses during leaf growth deduced from the data shown in graph h (**I**). For A to F and H, *n*=207.

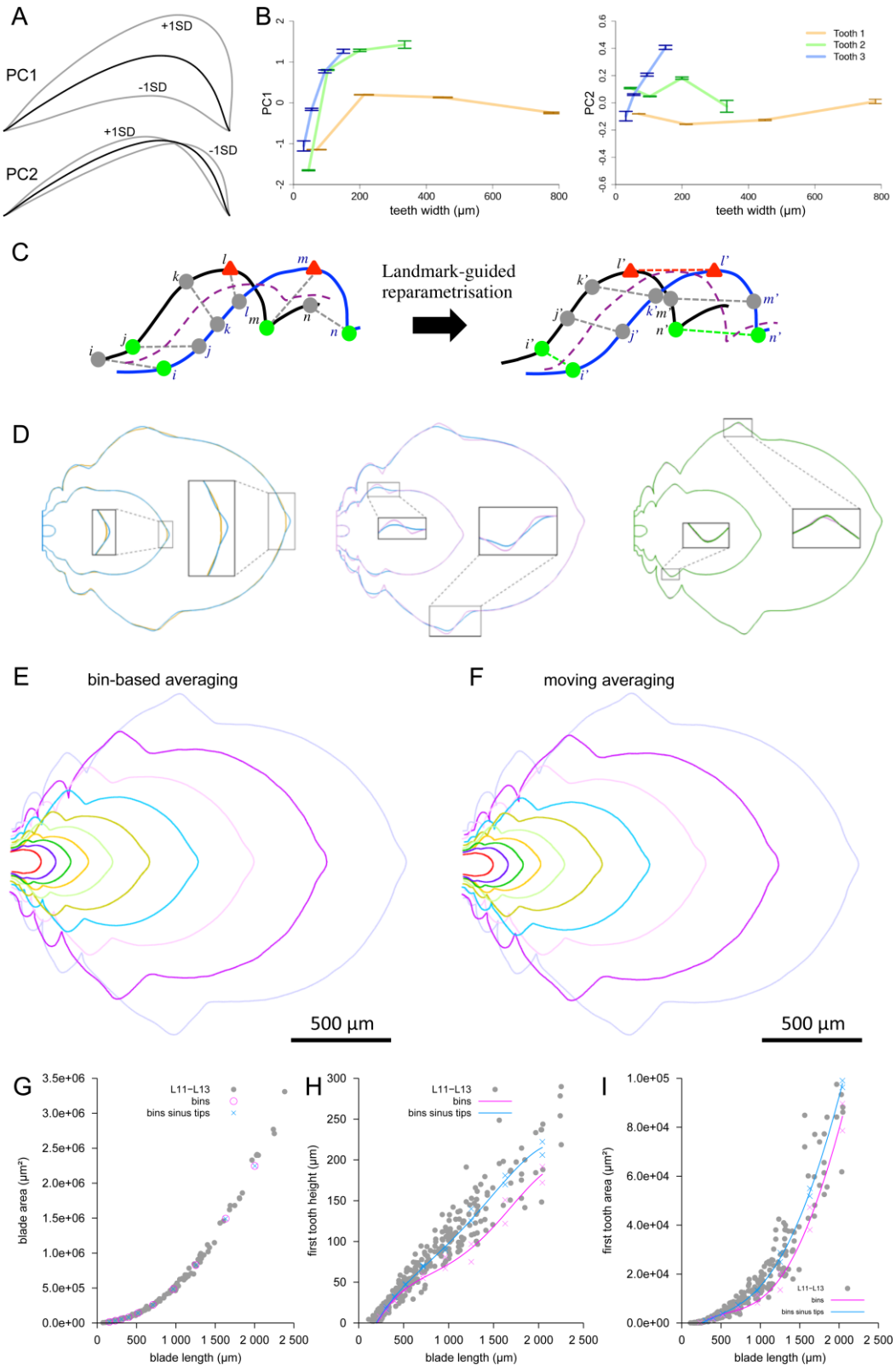


**Figure 3. Reconstruction of teeth and entire leaf developmental trajectory of L11-L13 using MorphoLeaf.**

(**A**,**B**). Principal Component analysis (PCA) of teeth shape (for teeth 1, 2 and 3). The mean shape is represented by a black line while the grey lines represent teeth shape obtained by varying the PC1 or PC2 value +/- 1 SD (**A**). Variations of PC1 and PC2 during the development of tooth 1, 2, or 3 for which tooth width was used as a proxy. PC1, which contributes to 91.2% of the total variability, corresponds to tooth height while PC2 (5.2% of total variability) corresponds to tooth asymmetry. Error bars represent SE (**B**). (**C**) Principle of the landmark-guided reparametrisation of the leaf contour. The leaf contour is defined by successive points, some of which correspond to biologically relevant landmarks such as sinuses (green dots) or tooth tips (red triangle). Averaging between different leaf contours (here the black and blue contours) involves averaging the positions of points along the curves with similar indices (for instance *i* or *j*). As points with similar indices do not necessarily correspond to homologous points along the contour, the resulting average contour (doted purple line) is artificially smoothed-out (left panel). After landmark-guided reparametrisation (right panel), homologous biologically relevant points are put into correspondence (here the tooth sinuses have a common index *i'* or *n'* and the tooth tips have a common index *l'*) while the same numbers of points are regularly positioned between homologous landmarks on each leaf contour. As a result, the average contour shows increased accuracy compared to the average contour obtained before reparametrisation. (**D**) Effect of increasing number of landmarks used to guide leaf contour reparametrisation. Mean leaf shapes obtained before reparametrisation (orange), using the leaf tip (blue), the leaf tip and the tooth sinuses (pink) or the leaf tip and the tooth sinuses and tips (blue) to guide the reparametrisation of the leaf contour. Using only the leaf tip as guiding landmark for reparametrisation not only improved the mean shape at the leaf tip but also improved tooth definition. Reparametrisation using in addition tooth sinuses had the strongest effect on the mean leaf shapes, as it led to a sharper definition of the sinuses and corrected most of the tooth erosion. If teeth tips were also added as guiding landmarks for the reparametrisation, the computed mean shape retrieved the small "hump" visible at the tip of older teeth. (**E**,**F**) Ten mean contours obtained after leaf tip, tooth sinuses and tooth tips guided reparametrisation and based either on bins defined on blade length (**E**) or on moving averaging (**F**). Note that the two methods generate similar mean shapes (**G-I**) Validation of the mean contours. Leaf area (**G**), height of the first tooth (**H**), or area of the first tooth (**I**) were plotted against blade length for both individual real leaves ("L11-L13", "first tooth", grey) and for the mean contour generated for the same 10 blade length classes as in (e), either before reparametrisation ("bins", purple) or following reparametrisation using leaf tips and tooth sinuses and tips ("bins sinus tips", blue).

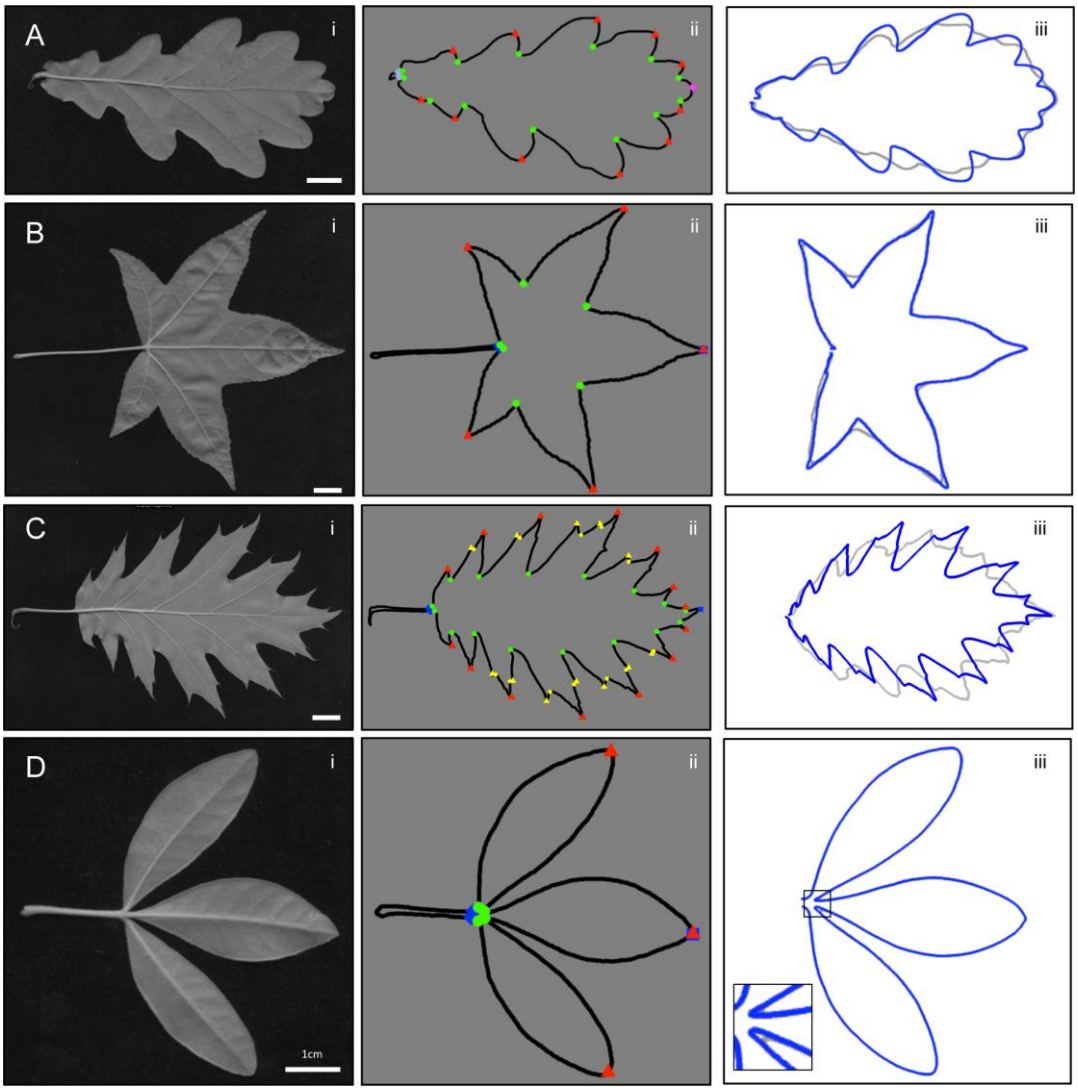


**Figure 4. Characterisation of mature leaf shapes of various species using MorphoLeaf**

MorphoLeaf was applied on a simple pinnately lobed leaf (sessile oak, *Quercus petraea*, **A**), a simple palmately lobed leaf (Maple, *Acer sp*, **B**), a simple pinnately lobed leaf with secondary structures (Northern red oak, *Quercus rubra*, **C**) and a palmately compound leaf (Mexican orange, *Choisya ternate*, **D**). For each species, a leaf (left panels, **i**), its contour with the biologically relevant landmarks (blue diamonds: petiole-blade junctions; blue cubes: leaf tips, green dots: primary tooth/lobe sinuses; red triangles: primary tooth/lobe tips; orange dots secondary tooth/lobe sinuses; orange triangles secondary tooth/lobe tips, central panels, **ii**) and mean contours (grey: generated without repametrisation; blue: generated after leaf tip, tooth sinuses and tips guided reparametrisation, right panels, **iii**) are shown. *n*=4 for the mean contours. The inset in **D iii** shows a detail of the base of the leaflets. Scale bars=1cm

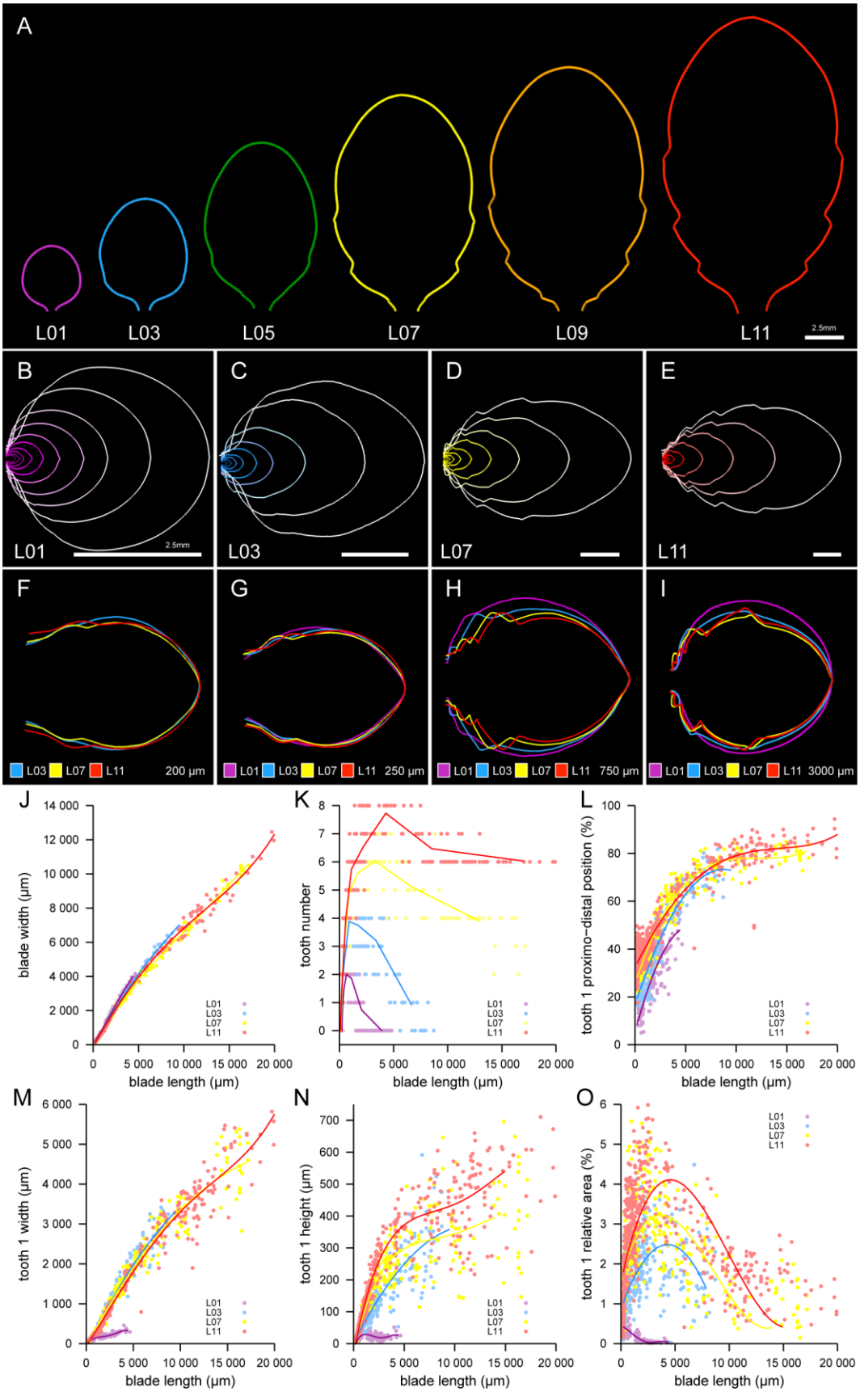
A
L01
L03
L05
L07
L09
L11
2.5mm
B
L01
2.5mm
C
L03
D
L07
E
L11
F
L03 L07 L11 200 µm
G
L01 L03 L07 L11 250 µm
H
L01 L03 L07 L11 750 µm
I
L01 L03 L07 L11 3000 µm
J
blade width (µm)
blade length (µm)
K
tooth number
blade length (µm)
L
tooth 1 proximo-distal position (%)
blade length (µm)
M
tooth 1 width (µm)
blade length (µm)
N
tooth 1 height (µm)
blade length (µm)
O
tooth 1 relative area (%)
blade length (µm)
L01
L03
L07
L11

**Figure 5. Morphometrics of developing Arabidopsis leaves of different rank, from their initiation to the mature stage using MorphoLeaf.**

(**A**) Mean shape of mature leaves L01, L03, L05, L07, L09 and L11 grown under short-day condition (*n*=10 for L01, L03, *n*=11 for L07, L09, L11 and *n*=12 for L05). (**B-E**) Developmental trajectories of L01 (**B**), L03 (**C**), L07 (**D**) and L11 (**E**). For each leaf 10 mean contours obtained by the normalisation method based on bins are represented (note the difference in scale between the panels). (**F-I**) Overlay of mean contours of different leaf primordia of 200 µm (**F**), 250 µm (**G**), 750 µm (**H**) and 3000 µm (**I**) obtained using the moving average normalization method. (**J-O**) Morphological parameters of L01, L03, L07, L011. Measures were performed on the whole leaf (**J, K**) or on tooth 1 (**L-O**). Blade width (**J**) and teeth number (**K**) plotted against blade length. Tooth position (**L**), tooth width (**M**), tooth height (**N**) and relative tooth area (area of the tooth/leaf area, **O**) are plotted against blade length. For the **B** to **O**, *n*=177 for L01, *n*=160 for L03, *n*=168 for L07 and *n*=312 for L11. Scale bars = 2.5mm

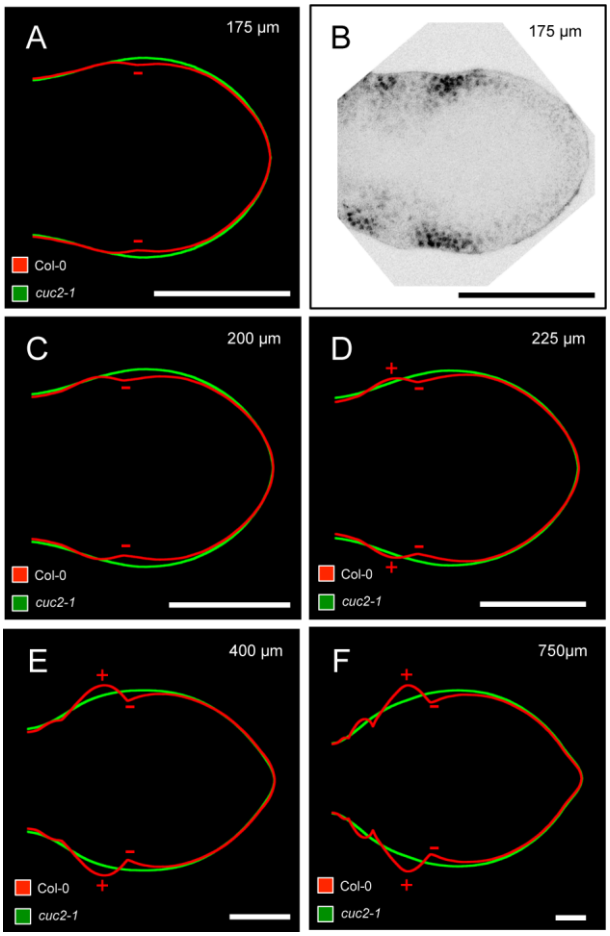


**Figure 6. Analysis of early stages of wild type and *cuc2-1* leaf development.**

(**A**, **C-F**) Average leaf primordium of wild type (red line) and *cuc2-1* (green line) at different sizes (indicated in the upper right corner in each panel). The "-" signs indicate zones where the wild type outline is less developed compared to the smooth *cuc2-1* outline while the "+" signs point to zones more developed in the wild type compared to *cuc2-1*. (**B**). CUC2:CUC2:VENUS expression (visible as black nuclei) in primordium at the stage as the one depicted in (a). Bars = 100 µm for all panels.

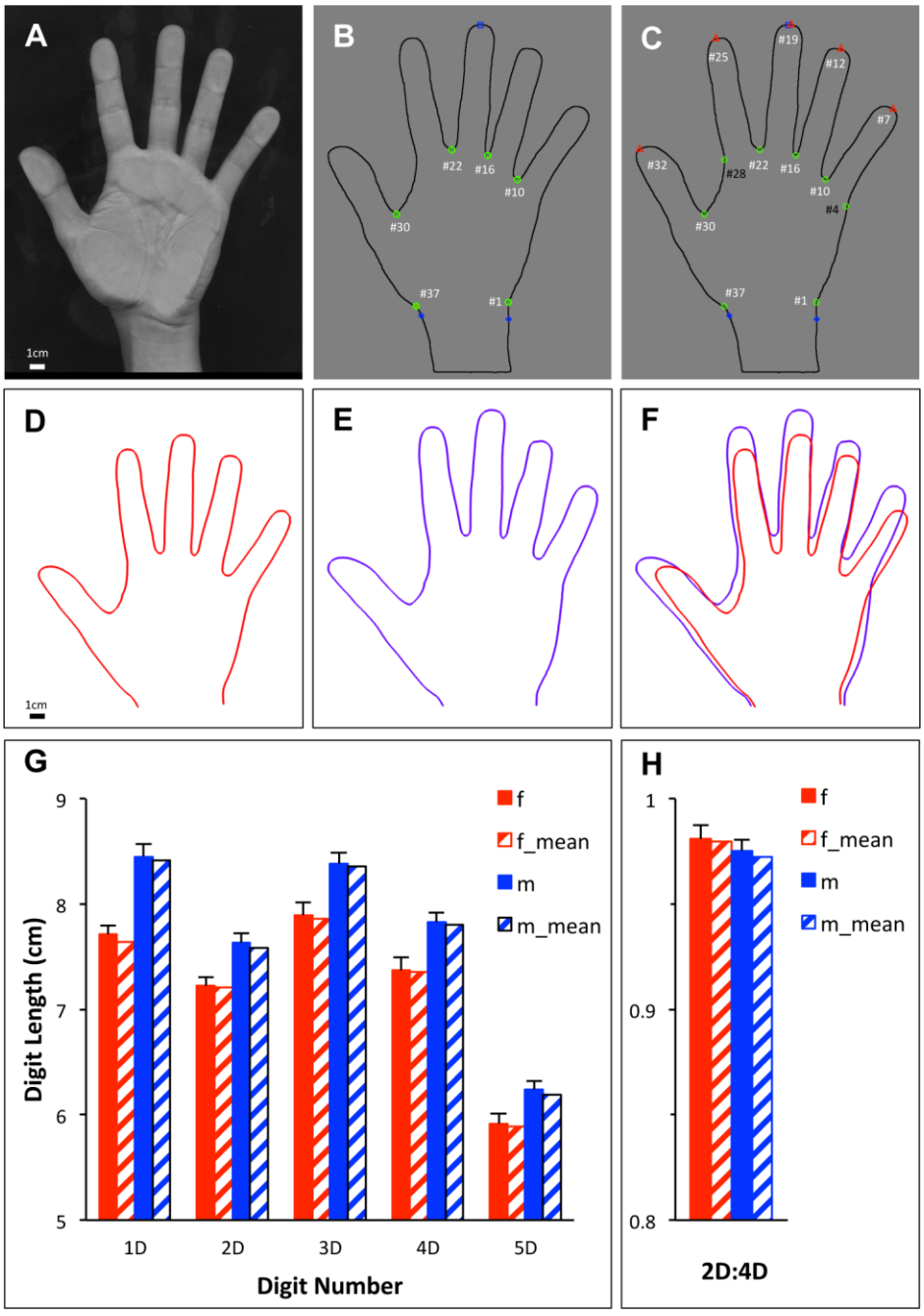


**Figure 7. Analysis of hand morphometrics using MorphoLeaf.**

(**A**) Left hand imaged with a scanner. (**B**) Result of automatic hand contour segmentation. The blue diamonds were manually placed and correspond to the limit between the hand and the arm. The green circles are the results of the automatic identification of the sinuses and allow the identifications of the landmarks #1, 10, 16, 22 and 37 described previously (Sanfilippo et al., 2013) (**C**). Two additional landmarks corresponding to landmarks #4 and 28 (Sanfilippo et

al., 2013) were manually added and the tips of the fingers automatically identified, thus providing the 5 additional landmarks #7, 12, 19, 25 and 32 (Sanfilippo et al., 2013) (**D**). Female average left hand reconstructed from 16 individuals. (**E**) Male average left hand reconstructed from 12 individuals. (**F**) Overlay of the average female (red) and male (blue) left hand. Scale bars: 1 cm (**G**) Digit length (digit numbered from 1 to 5 from the thumb to the little finger). Solid red and blue bars represent the means of the measures made by MorphoLeaf on female and male individuals, respectively while the hatched bars represent the measures made on the mean shapes reconstructed by MorphoLeaf and shown in (d) and (e) Error bars are SE. (**H**) Ratio between the length of digit 2 (2D) and digit 4 (4D). Solid red and blue bars represent the means of the 2D:4D ratio of the measures made by MorphoLeaf on female and male individuals, respectively while the hatched bars represent the 2D:4D ratio of the measures made on the mean shapes reconstructed by MorphoLeaf and shown in (d) and (e). Error bars are SE.

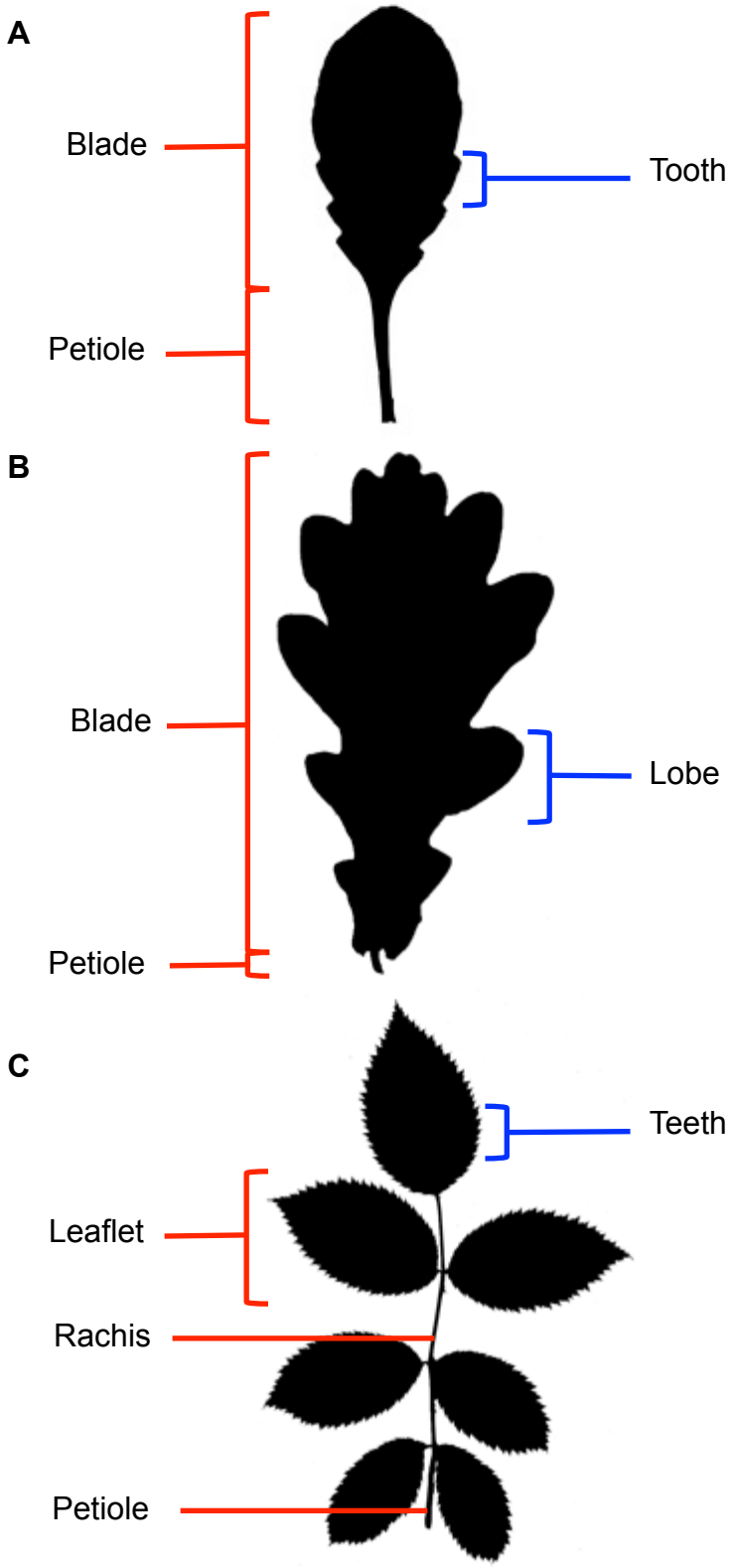


**Supplementary Figure S1. Basics of leaf architecture.**
Silhouette of an *Arabidopsis thaliana* (**A**), sessile oak (**B**) and rose (**C**) leaf. The Arabidopsis and sessile oak leaves are simple leaves formed by a petiole supporting a single leaf blade which margin is dissected into small teeth in the case of Arabidopsis and larger lobes in the case of sessile oak. Rose has a compound leaf formed by several leaflets united by the rachis. The margin of the leaflets are dissected into numerous tiny serrations.

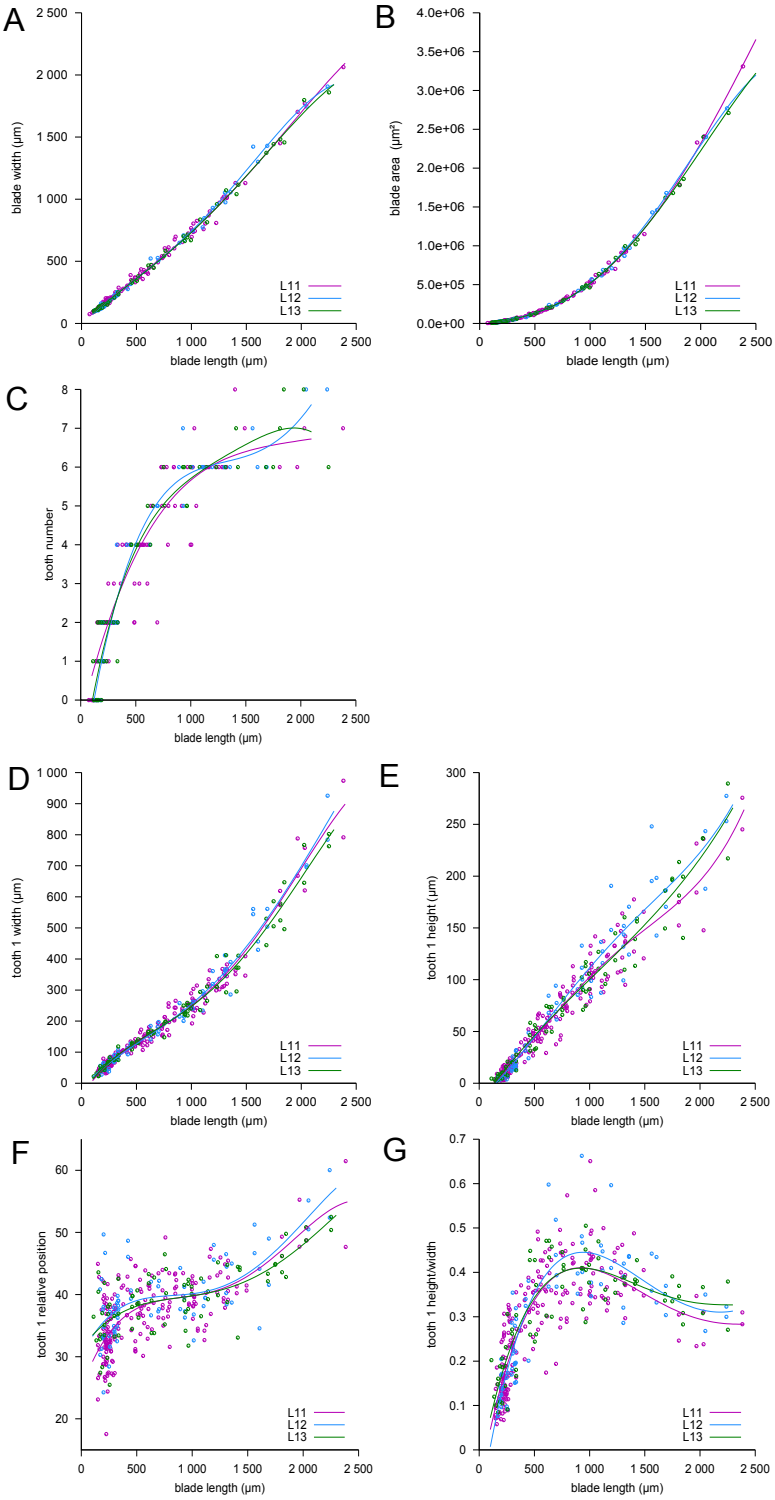


**Supplementary Figure S2. Morphometrics of leaves L11, L12 and L13.**
Morphological parameters were extracted for young leaves L11, L12 and 13 based on biologically relevant landmarks determined by the MorphoLeaf application. Measures were performed on the whole leaf (**A-C**) or on tooth 1 (**D-G**, teeth numbered according to their position on each side of the leaf blade starting from the tip to the base, which also correspond to their order of initiation). Blade width (**A**), blade area (**B**) and teeth number (**C**) plotted against blade length. Tooth width (**D**), tooth height (**E**), relative proximo-distal position of the distal sinus of teeth 1 (**F**) and tooth height to width ratio (**G**) plotted against blade length. *n*=114 for L11, *n*=46 for L12 and *n*=47 for L13

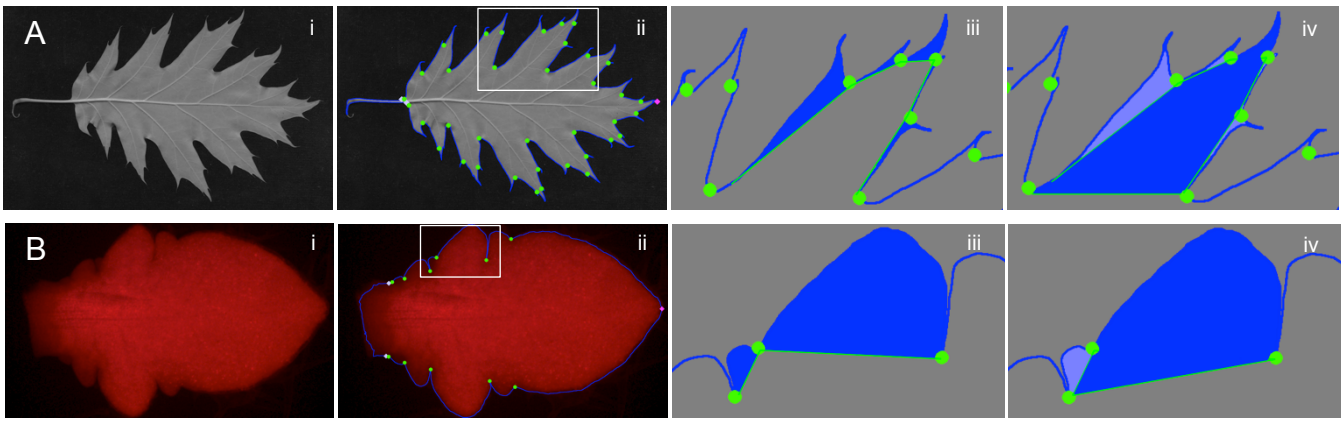


**Supplementary Figure S3. Hierarchical organisation of leaf margin outgrowths.**
The hierarchical organisation of the leaf margin in northern red oak (*Quercus rubra*, **A**) and *Arabidopsis thaliana* (**B**). The first panels (**i**) show the leaves, the second panels (**ii**) show the results of the segmentation and landmark identification (junctions between the petiole and the blade (grey diamonds), leaf tip (pink diamond) and sinuses (green dots)). The third panels (**iii**) show the results of the naive identification of the teeth (in blue) as structures contained between two successive sinuses. The fourth panels (**iv**) show the correct identification of the teeth, with secondary structures (light blue) supported by first order teeth (blue). Note that the whole tooth corresponds to light blue and blue regions.

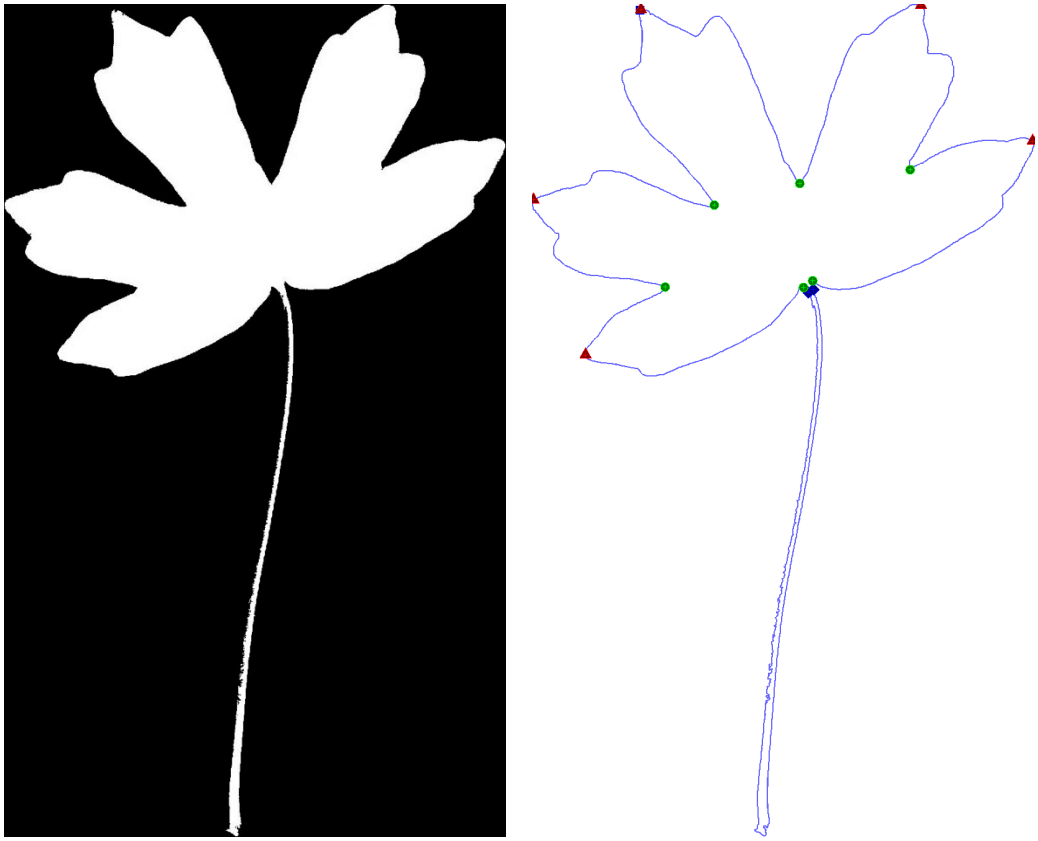

*Acer campestre*

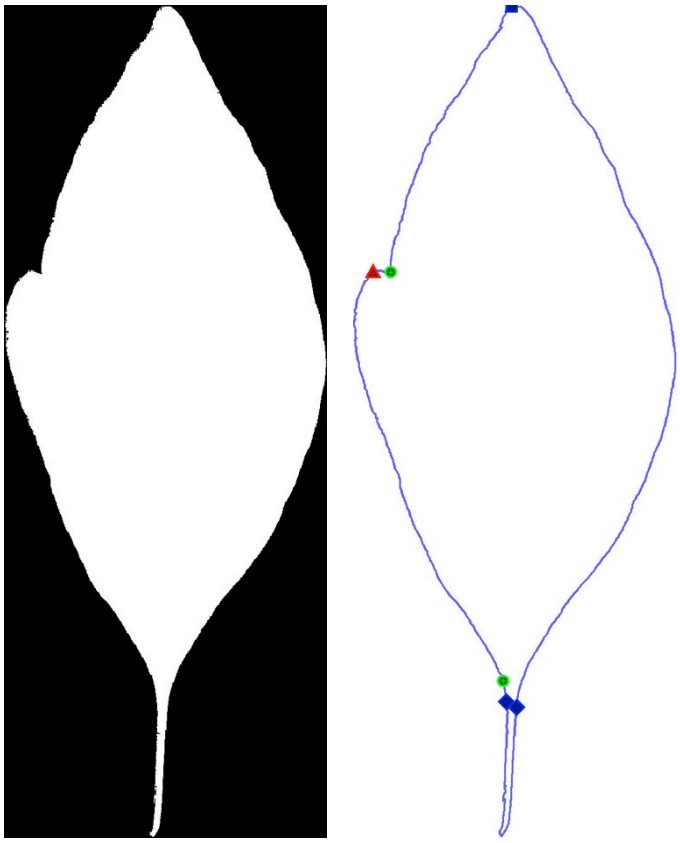

*Acer negundo*

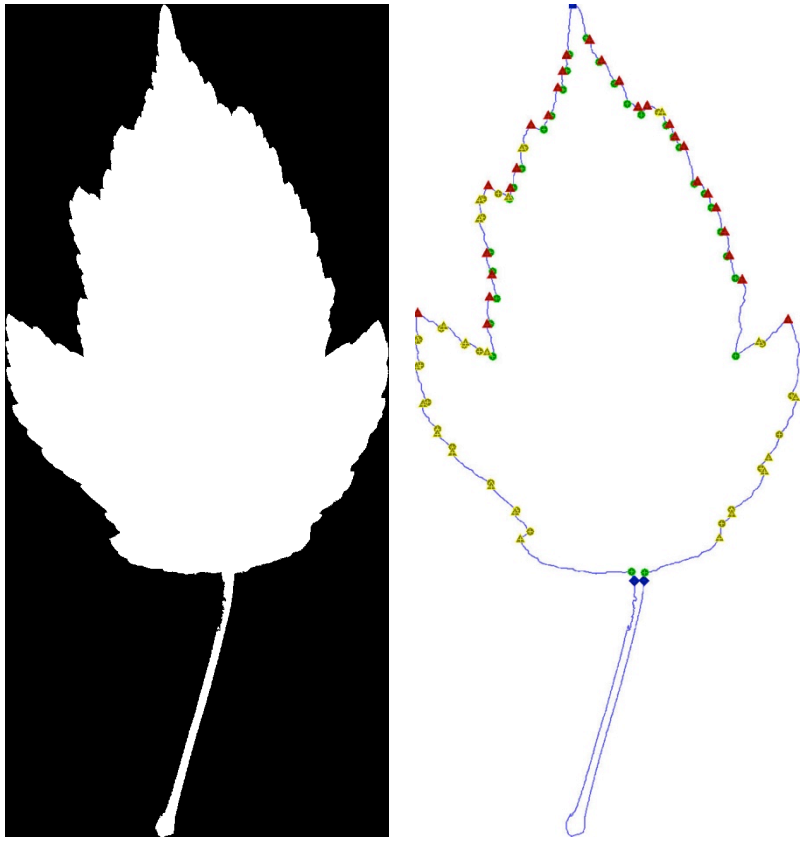

*Acer tataricum*

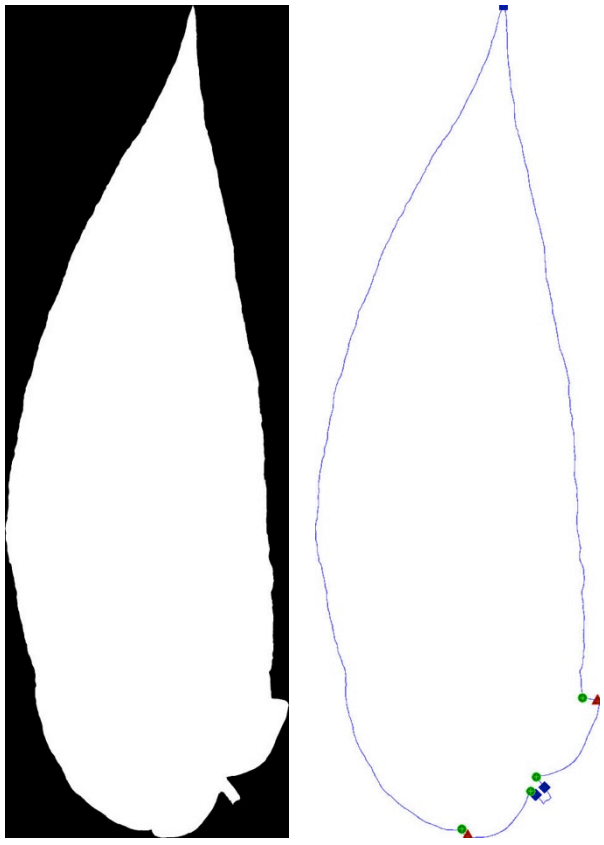

*Ailanthus altissima*

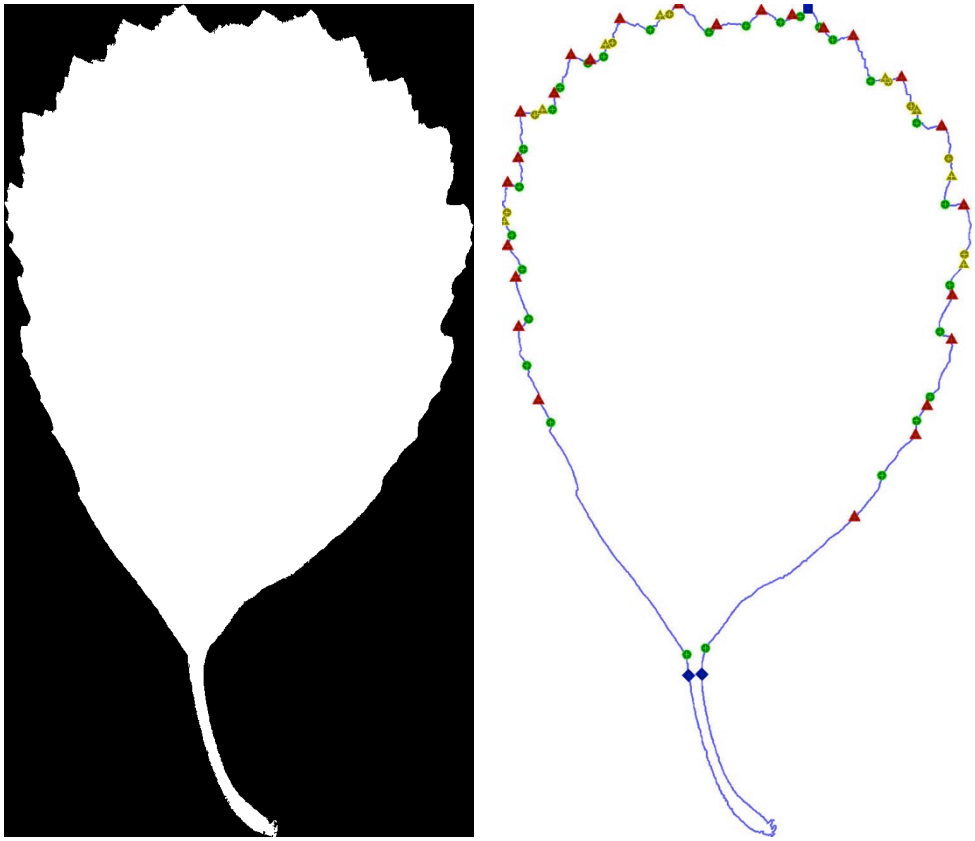

*Alnus glutinosa*

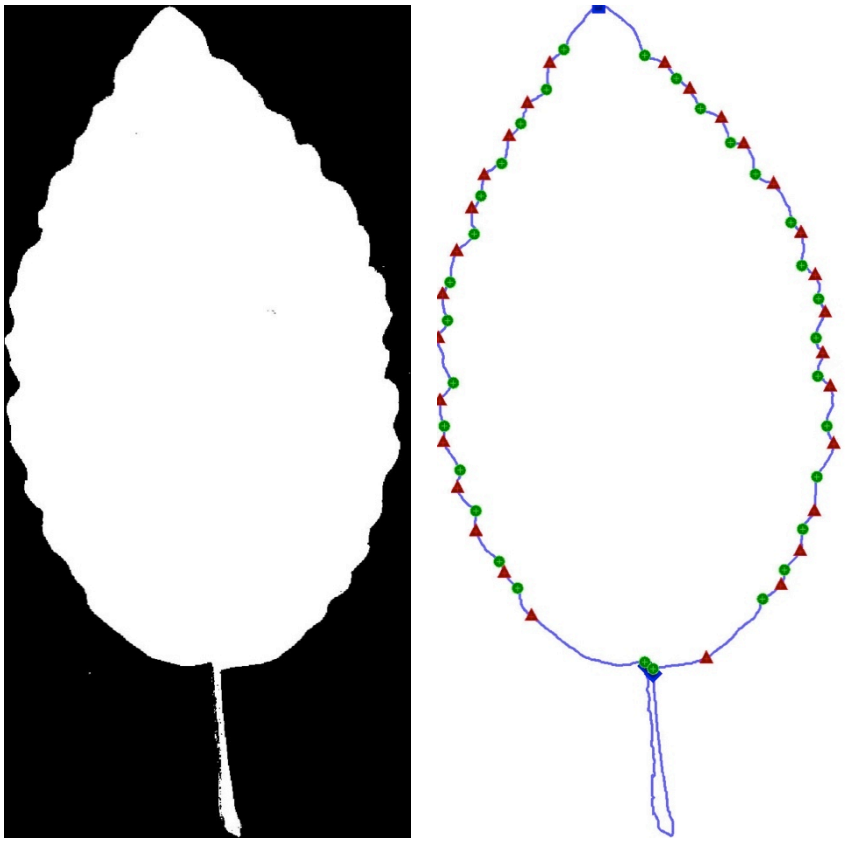

*Alnus orientalis*

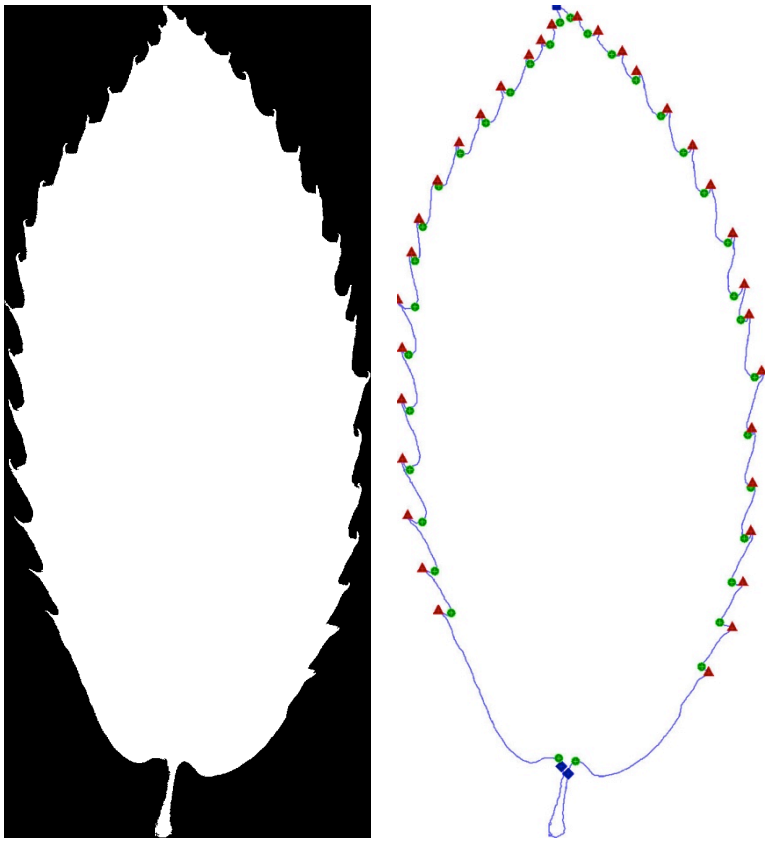

*Castanea sativa*

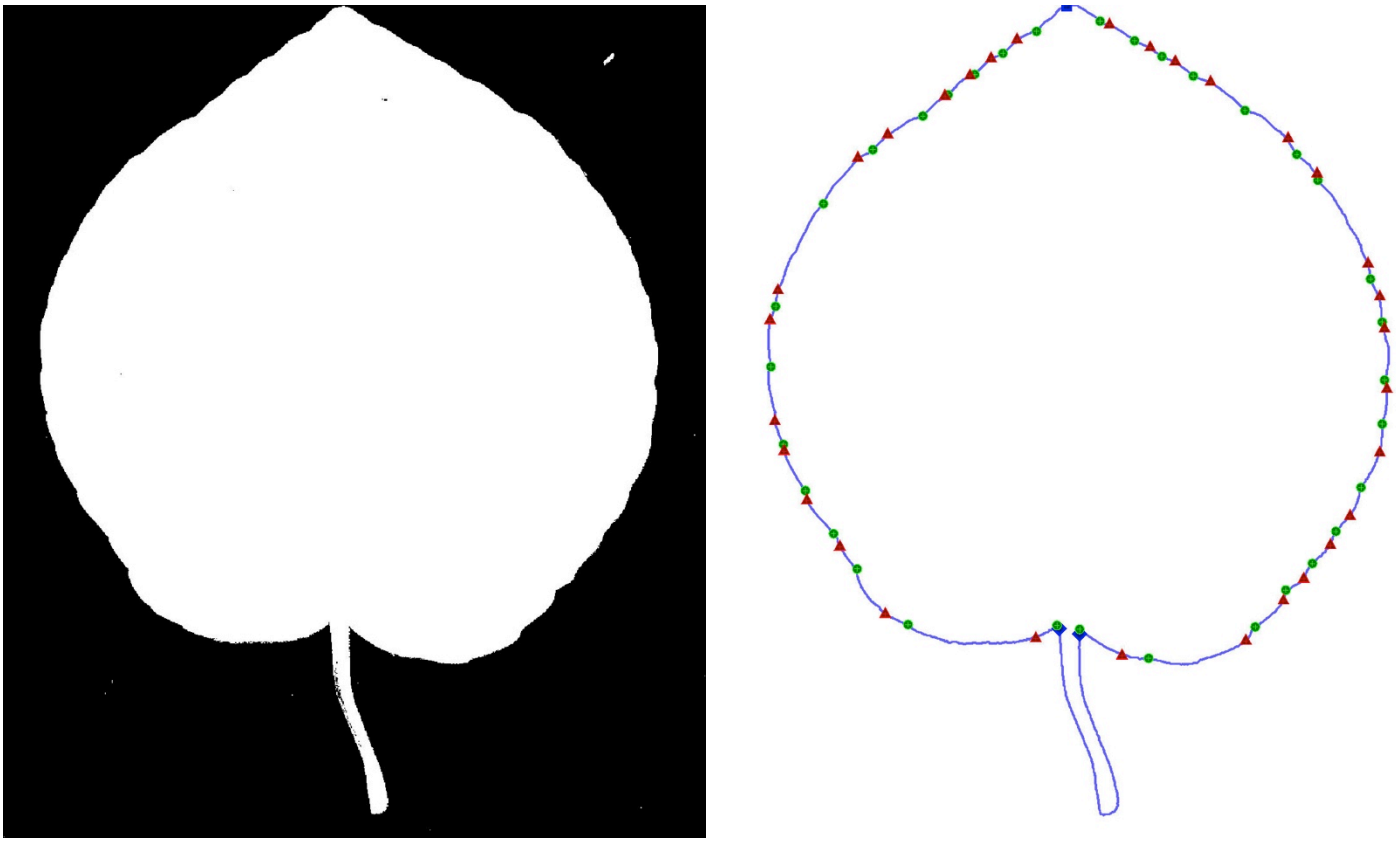

*Cercidiphyllum japonicum*

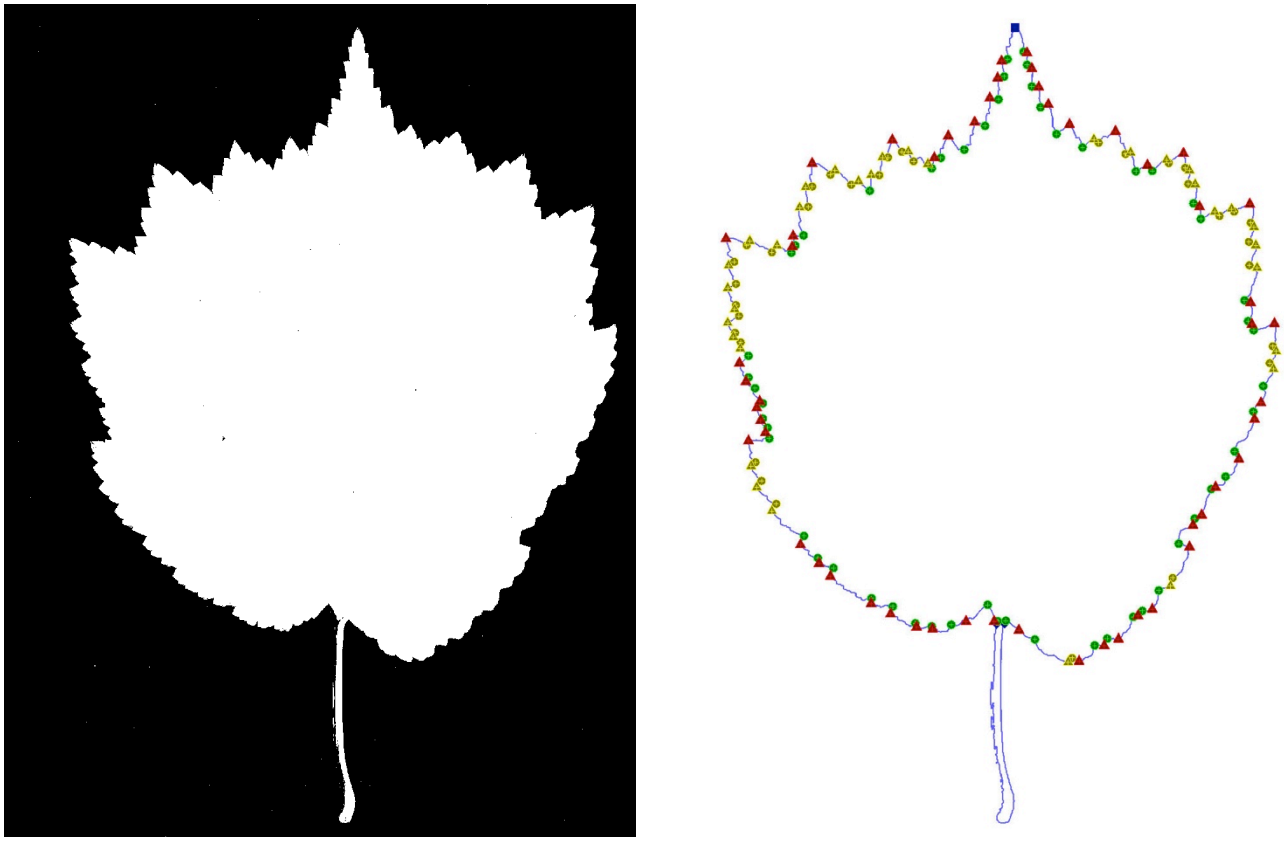

*Corylus colurna*

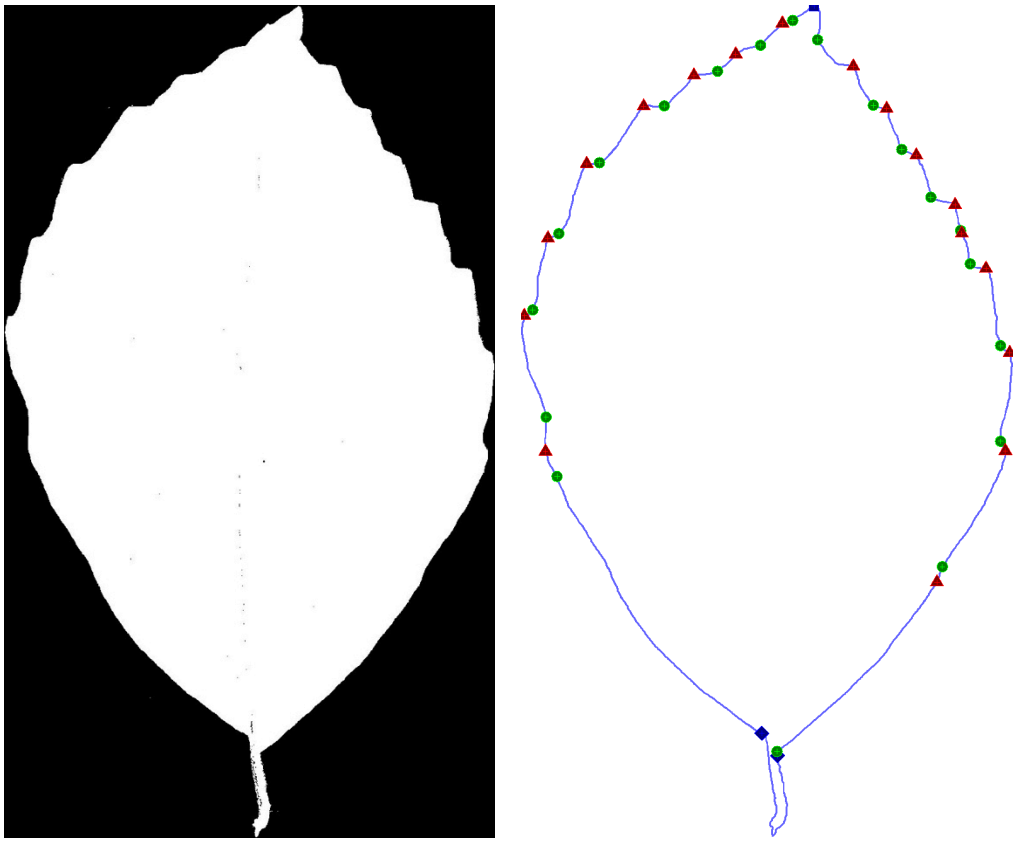

*Fagus sylvatica*

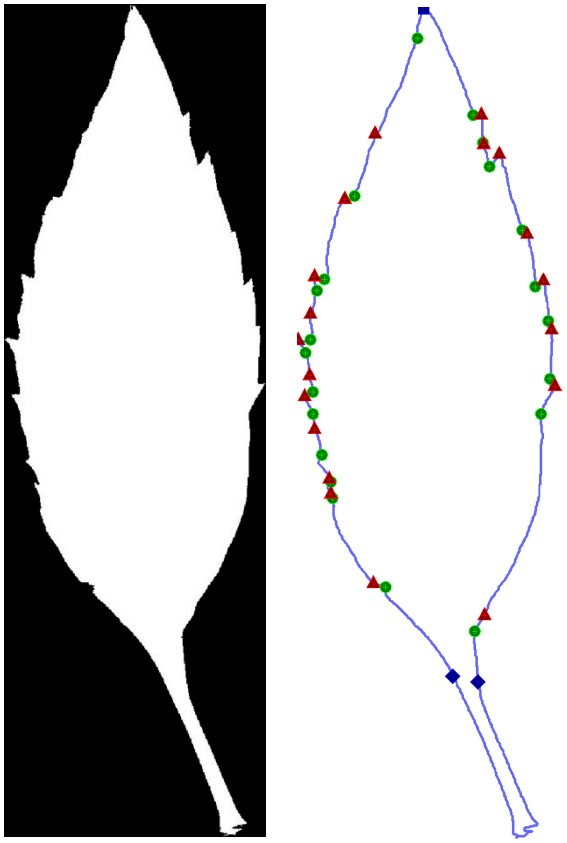

*Forsythia intermedia*

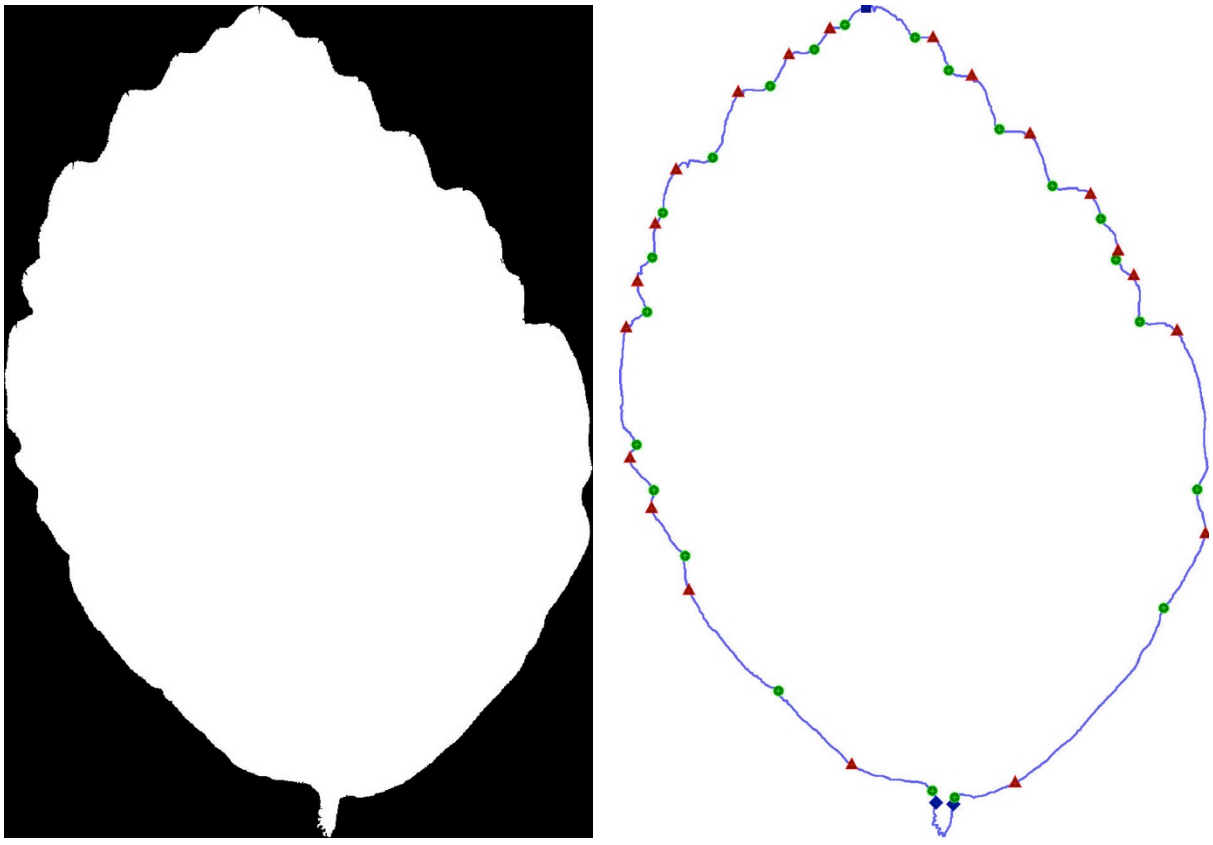

*Hamamelis japonica*

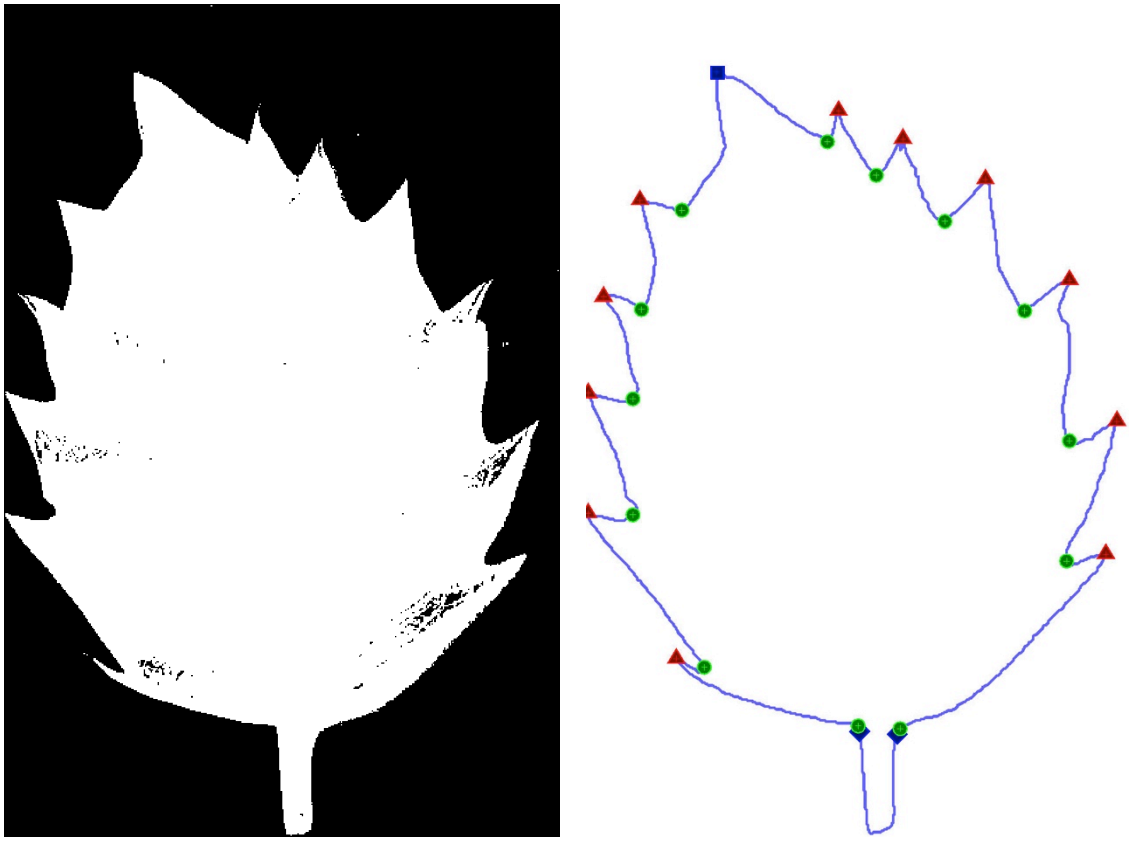

*Ilex aquifolium*

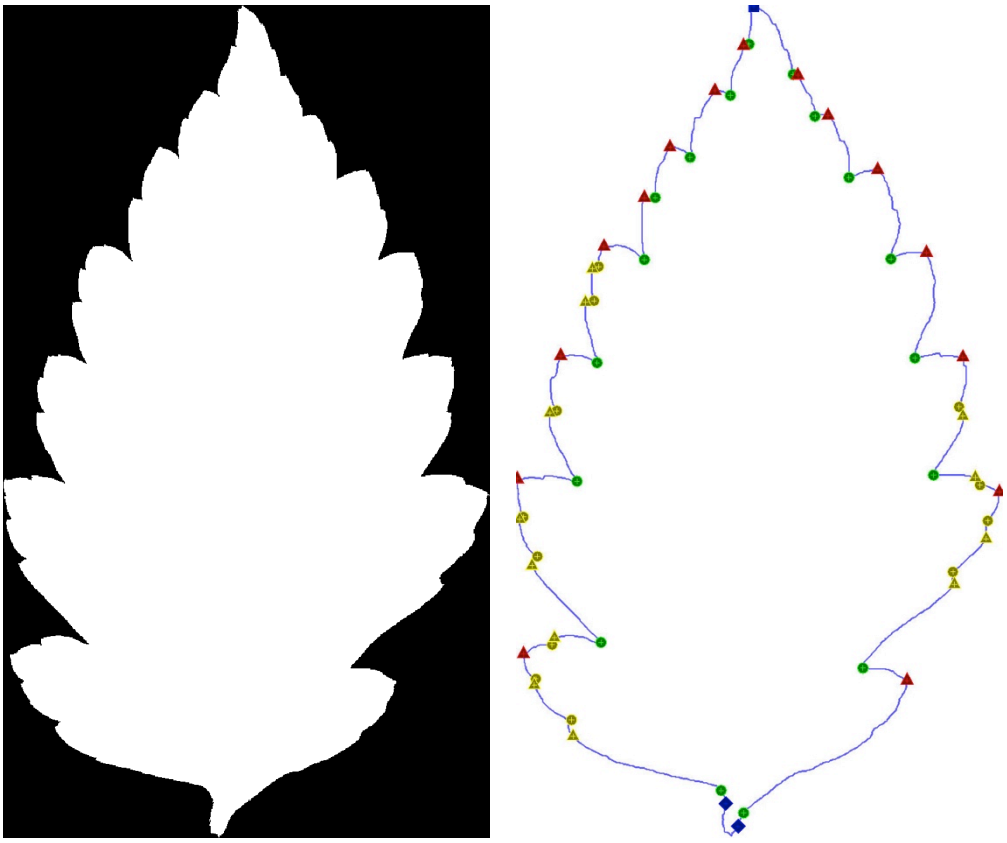

*Koelreuteria paniculata*

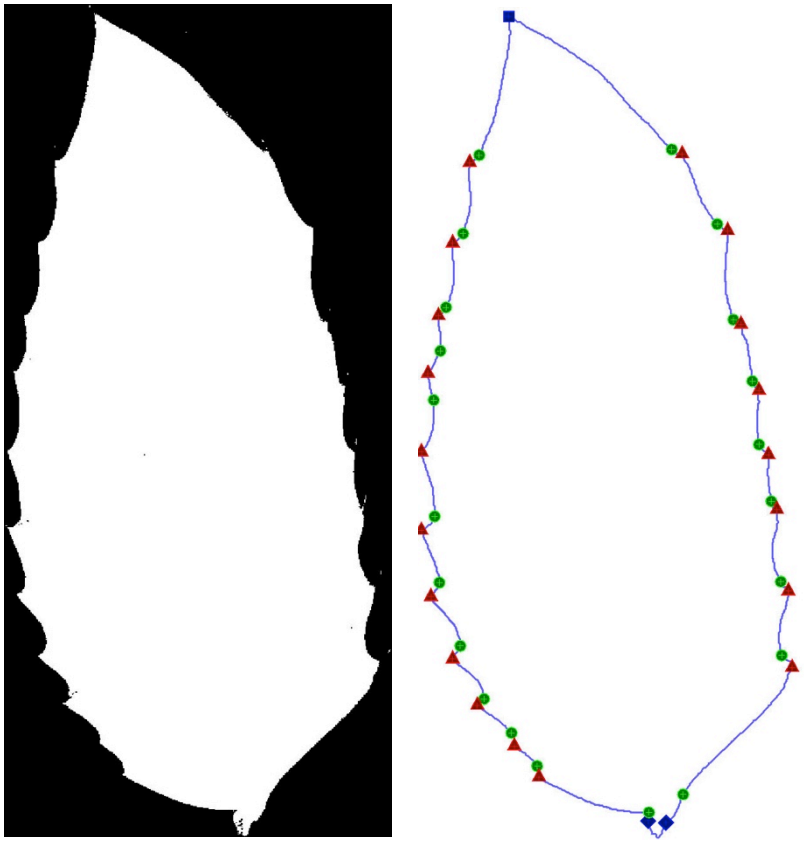

*Mahonia aquifolium*

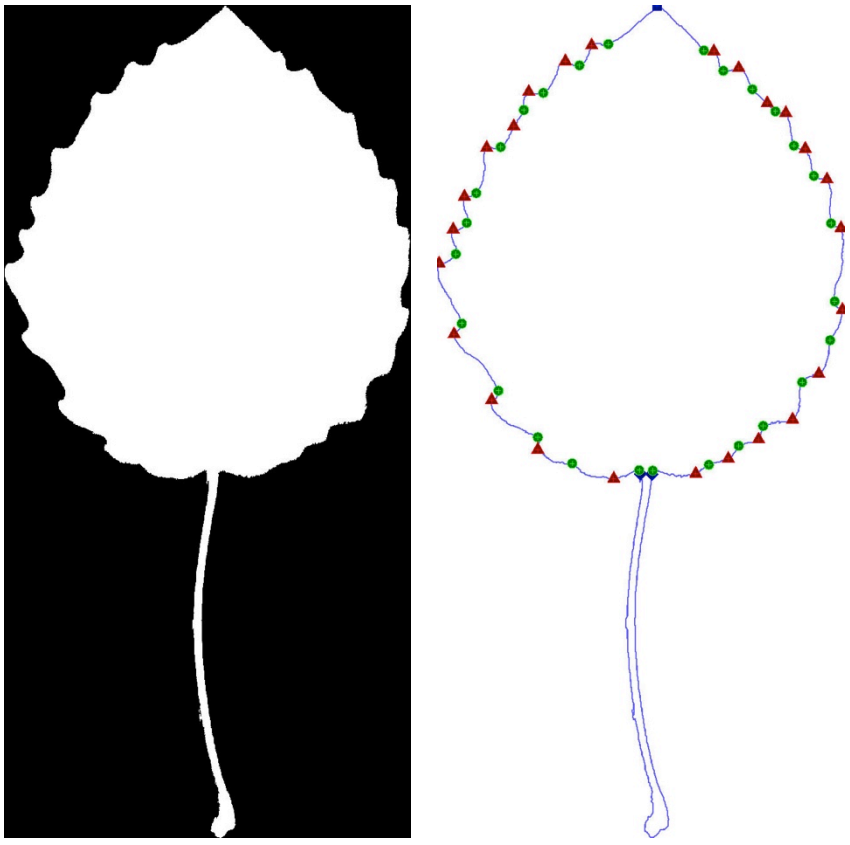

*Populus tremula*

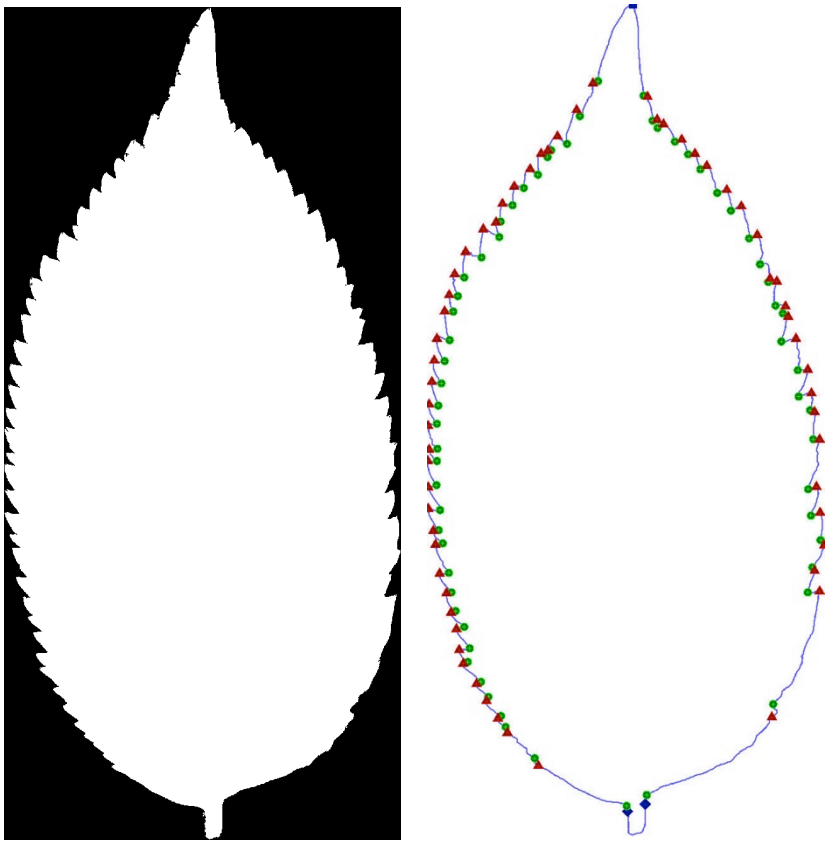

*Sambucus nigra*

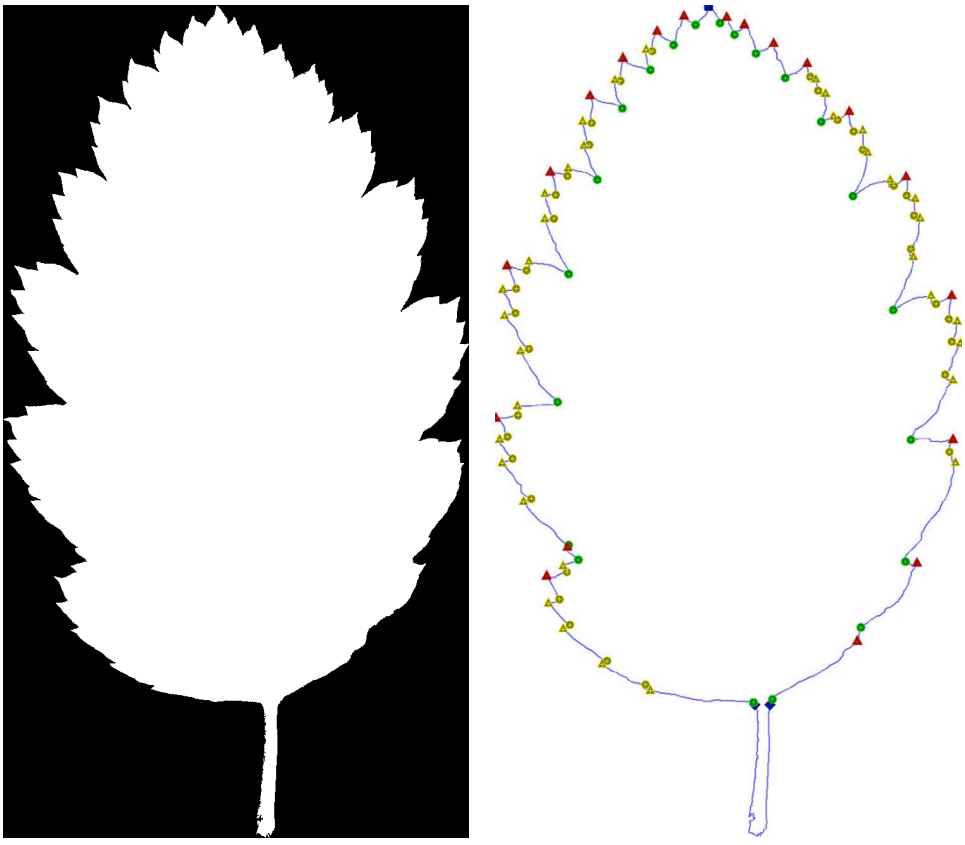

*Sorbus intermedia*

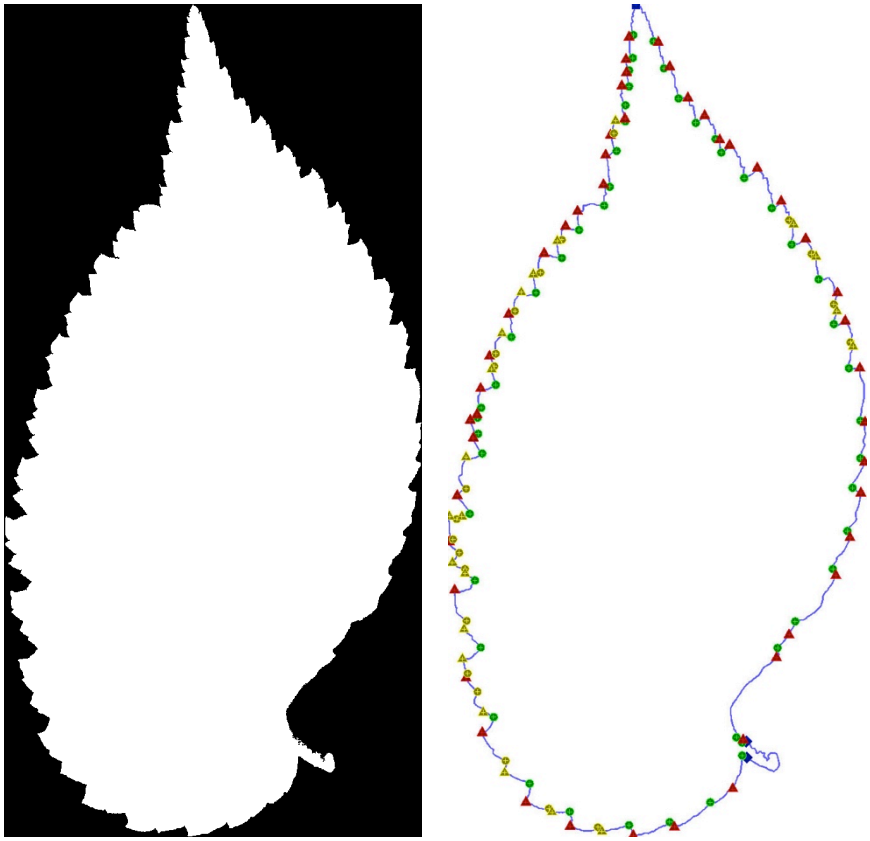

*Ulmus laevis*

**Supplementary Figure S4. Analysis of leaf shape of different species using MorphoLeaf.**
For each species, the input leaf image (binary image, left panel) and the result of the analysis performed with MorphoLeaf (right panel) are shown. Note that no manual corrections have been done, and that the results shown are those directly obtained by the MorphoLeaf.
Landmark description: blue diamonds: petiole-blade junctions; blue cubes: leaf tips, green dots: primary tooth/lobe sinuses; red triangles: primary tooth/lobe tips; orange dots secondary tooth/lobe sinuses; orange triangles secondary tooth/lobe tips.
The leaf pictures are from the Middle European Woods data base from the Department of Image Processing at the Institute of Information Theory and Automation of the ASCR, Czech Republic.

**Novotný, P. and Suk,** T. (2013) Leaf recognition of woody species in Central Europe. *Biosys. Eng*. **115**, 444-452.

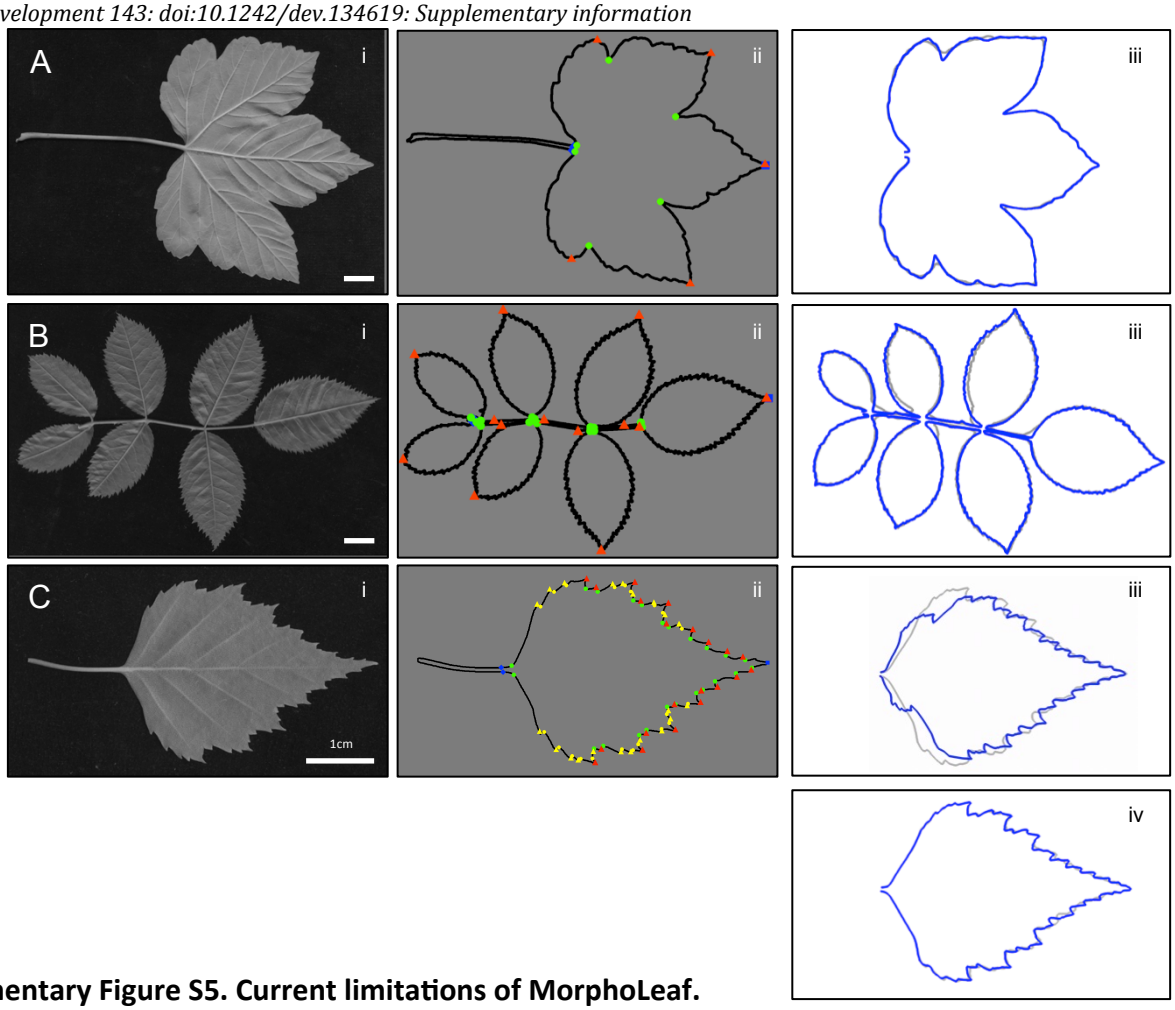


**Supplementary Figure S5. Current limitations of MorphoLeaf.**

For each species, a leaf (left panels, **i**), its contour with the biologically relevant landmarks (blue diamonds: petiole-blade junctions; blue cubes: leaf tips, green dots: primary tooth/lobe sinuses; red triangles: primary tooth/lobe tips; orange dots secondary tooth/lobe sinuses; orange triangles secondary tooth/lobe tips, central panels, **ii**) and mean contours (grey: generated without reparametrisation; blue: generated after leaf tip, tooth sinuses and tips guided reparametrisation, right panels, **iii**) are shown. Scale bars=1cm

The hierarchy of palmately lobed leaves with several levels of dissection (such as sycamore maple, *Acer pseudoplatanus* **A-i**) cannot be established with MorphoLeaf. Nevertheless, appropriate setting of the parameters allows the detection of the sinuses on the main lobes (**A-ii**) and thus proper quantitative analyses and mean leaf shape reconstruction (**A-iii,** *n*=4).

In MorphoLeaf two neighbouring structures such as teeth or lobes share the same sinus between them. Because of this definition the MorphoLeaf cannot be used to properly analyse pinnately compound leaves (such as rose, *Rosa* sp, **B-i**), in which two neighbouring leaflets are separated by a stretch of the rachis. Running MorphoLeaf leads to the identification of extra structures corresponding to rachis segments (**B-ii**) and hence producing false quantitative analyses. Nevertheless, the mean shape that is reconstructed by MorphoLeaf is accurate (**B-iii**, *n*=3).

MorphoLeaf allows the identification of complex patterns of dissections (such as those of European white birch, *Betula pendula*, **C-i** and **C-ii**). However, while using the primary sinuses and peaks to guide the reconstruction increases the quality of the mean shape in the distal part of the leaf, it degrades the quality in the proximal part (compare grey and blue contours in **C-iii**, *n*=3). Because of the heterogeneity in the sizes of primary teeth (alternatively large and small teeth in the proximal region of the leaf) and the variability in the total number of teeth (10 or 11 per half-leaf here), dissimilar structures are put into correspondence to reconstruct the mean shape. To avoid this, the user can manually homogenise the number of teeth per half leaf on each sample (by adding or removing teeth in the distal part where they are small), which solves the homology issue and leads to an accurate reconstruction of the mean shape in both the distal and proximal part of the leaf (**C-iv**).

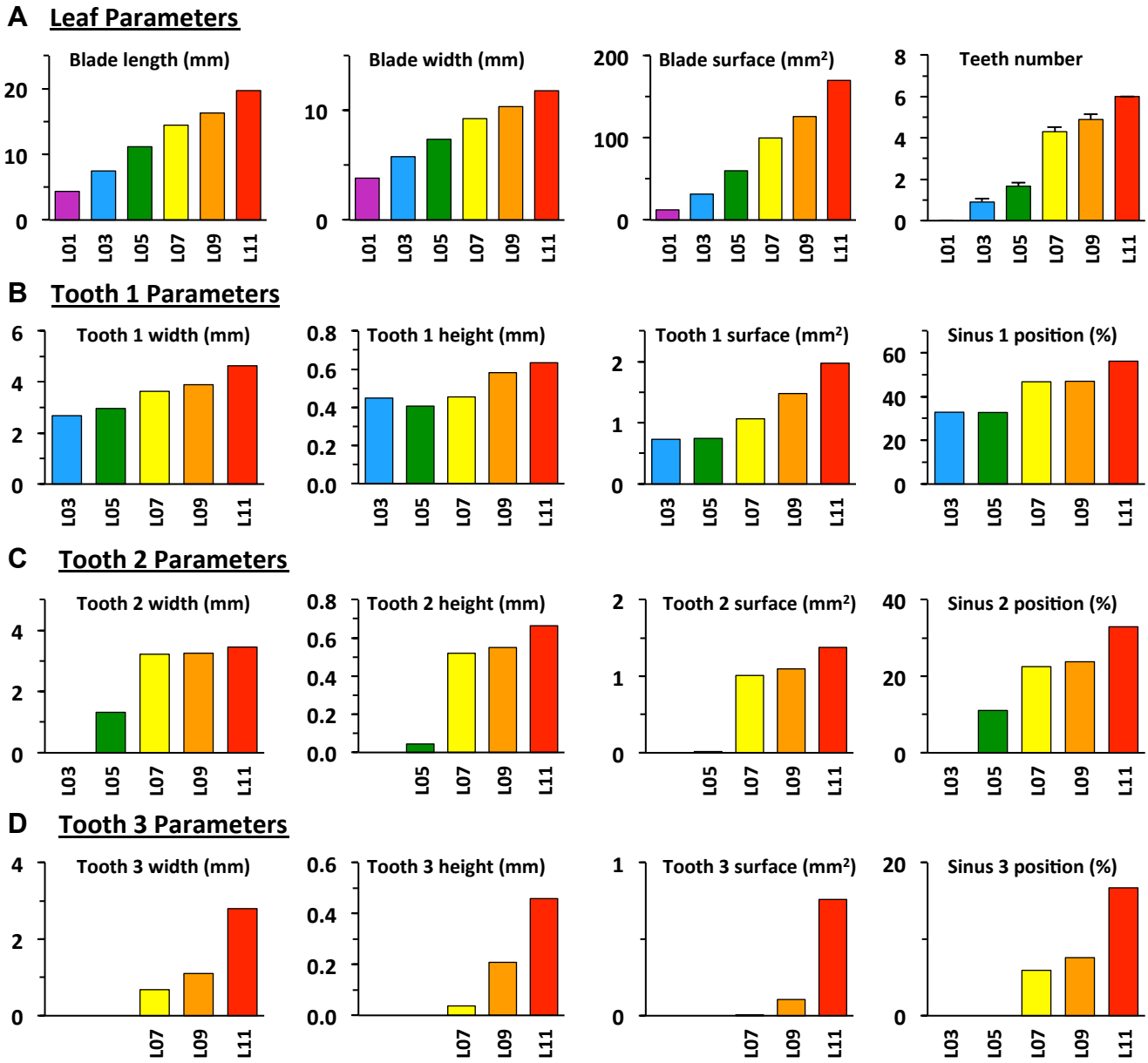


**Supplementary Figure S6. Morphometrics of mature leaves L01, L03, L05, L07, L09 and L11.**
(**A**) Quantitative parameters associated with the entire leaf. All these parameters (except the teeth number) were determined on the reconstructed mean shapes. The number of teeth was calculated from the leaves that were used to generate the mean shapes, error bars are standard errors. (**B,C,D**) Quantitative parameters associated with tooth 1, 2 and 3 determined from the reconstructed mean shapes. *n*=10 for L01, L03, *n*=11 for L07, L09, L11 and *n*=12 for L05.

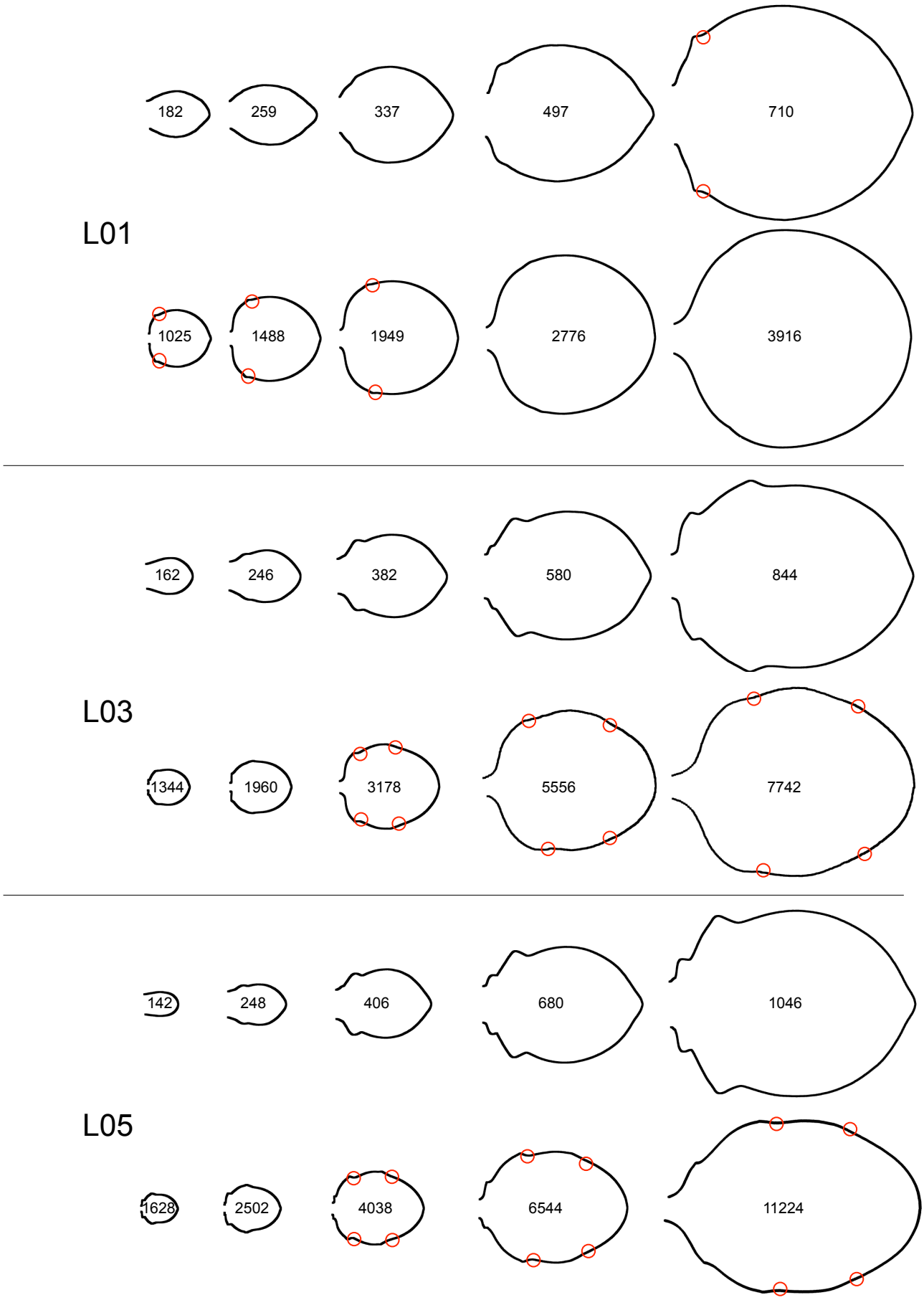


138
272
412
670
1102
L07
1786
3042
4838
8042
12056
158
262
438
718
1210
L09
1940
3150
5234
10008
16206
152
256
476
714
1186
L11
2126
3984
6992
11168
17770

**Supplementary Figure S7. Developmental trajectories of leaf L01, L03, L05, L07, L09 and L11**
For each leaf rank (L01, L03, L05, L07, L09 and L11), 10 mean shapes were reconstructed using the normalization method based on bins are shown. For each leaf, the first five mean shapes and last five mean shapes are at the same scale. The blade length (in µm) of the mean shapes is indicated inside of the contours. The tooth sinuses that become shallower during later stages of development and are hardly detectable at the mature stage are circled in red.

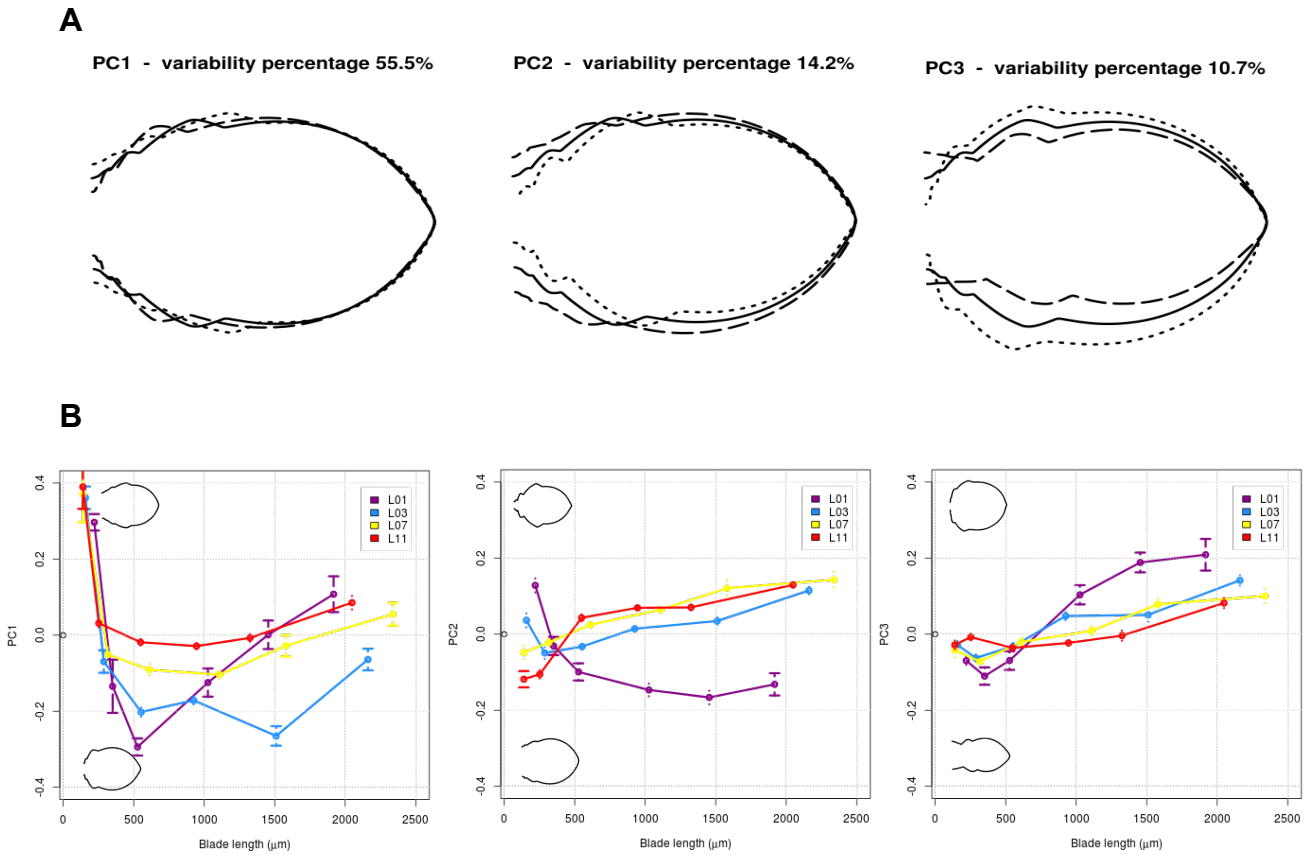


**Supplementary Figure S8. PCA Analysis of L01, L03, L07 and L11**

(**A**) PCA analysis of the whole sample of registered and reparametrised leaf contours (between 100 and 2000 µm). The mean shape is represented by a solid line while fine and gross doted lines represent leaf shapes obtained by varying the PC by + 1SD and -1SD, respectively. This analysis identified three principal components that explained more than 80% of the total shape variability. The first axis (PC1, 55,5% of total variability) may be interpreted as corresponding mostly to differences in teeth positions along the proximo-distal axis of the leaf. The second axis (PC2, 14% of total variability) may be linked to the size of the teeth. The third axis (PC3, 11% of total variability) may correspond to a global shape feature.

(**B**) Variations of PC1, PC2 and PC3 during the course of leaf development (error bars are standard errors).

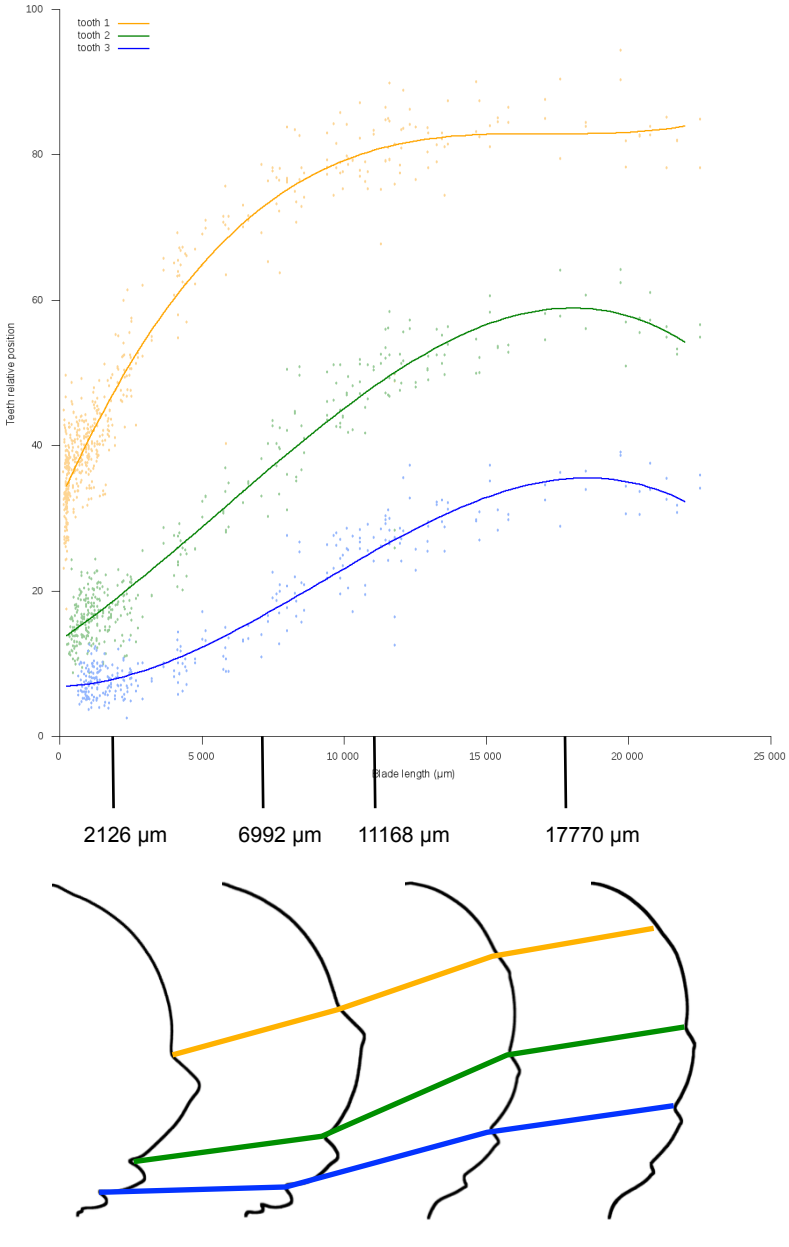


**Supplementary Figure S9. Relative position of teeth 1, 2 and 3 sinus along the proximo-distal leaf axis during entire L11 development.**

The relative position of the distal sinus of teeth 1, 2, and 3 along the proximo-distal axis of the leaf is shown during the entire development of L11. Below, three size-fitted average shapes at four different developmental stages are shown and the trajectories of the distal sinuses of teeth 1, 2 and 3 are indicated using the same colour code as in the graph. The region of the leaf located between the distal sinus of tooth 3 (blue line) and the base of the leaf is the region which shows the strongest relative increase in size during the development of leaves > 2 mm in length.

| | | Leaf Shape | | | | | | | | |
|---|---|---|---|---|---|---|---|---|---|---|
| | | **lanceolate** | **elliptical** | **ovate** | **obovate** | **cordate** | **palmate** | **lobed** | **palmately compound** | **pinnately compound** |
| **Margin Shape** | **smooth** | | | | | | | | *Choisya ternate* | |
| | **denticulate** | | *Sambucus nigra* | | | | *Acer sp.* | | | *Rosa sp* |
| | **crenate** | | | *Alnus orientalis* | | | | | | |
| | **sinuate** | | *Hamamelis japonica* | *Populus tremula* | | *Cercidiphyllum japonicum* | | | | |
| | **serrate** | *Forsythia intermedia* | *Arabidopsis thaliana*<br>*Fagus sylvatica*<br>*Mahonia aquifolium* | *Ilex aquifolium* | | | *Acer pseudoplatanus* | | | |
| | **spiny** | | *Castanea sativa* | | | | | | | |
| | **lobate** | *Acer negundo*<br>*Ailanthus altissima* | | | | | *Acer campestre* | *Quercus petraea* | | |
| | **lobate serrate** | | | *Koelreuteria paniculata* | | | | *Acer tataricum* | | |
| | **doubly dentate** | | | | *Alnus glutinosa* | *Corylus colurna* | | | | |
| | **doubly serrate** | | *Betula pendula* | *Sorbus intermedia* | | *Ulmus laevis* | | *Quercus rubra* | | |

**Table S1. Summary of the species analysed.** For each species the leaf shape and the margin shape are indicated

# Supplementary Methods

## MorphoLeaf software methods

### Blade contour segmentation and landmark detection

*Leaf contour segmentation*

On each image of a data set, the contour of the leaf is automatically extracted using the watershed method (Vincent and Soille, 1991). Briefly, two markers are located on the image, one within the leaf area and one within the background. These markers are obtained after an automated thresholding of the image intensities, which allows to roughly separate the regions corresponding to the leaf and the background. Then, the watershed algorithm allows to efficiently detect the limit of the leaf (Figure SM1, contour in yellow). In order to remove non-relevant details along the contour, the MorphoLeaf application proposes a tool to simplify the contour. This simplification is performed by retaining only the first elliptical Fourier descriptors that encode the contour in the frequency domain (Kuhl and Giardina, 1982). In the MorphoLeaf application, the number of descriptors (i.e. the degree of simplification) is controlled by the "*Fidelity*" parameter, which corresponds to the proportion of the power spectrum that must be retained during the simplification .

*Leaf blade identification*

Once the leaf contour is extracted, the limit between the petiole and the blade is manually determined by the user. This is not automated due to the difficulty to find a common criterion to various species and developmental stages. In practice, the user sets two landmarks on the contour on both sides of the petiole-blade limit. The blade is then defined as the half contour on either side of the *Petiole* landmarks that defines the largest area (the other one, which corresponds to the petiole of the leaf, is not further analyzed). Next, the leaf apex is automatically determined as the position on the blade contour that is at the maximal Euclidean distance from the midpoint of the segment defined by the petiole landmarks (see Figure SM1).

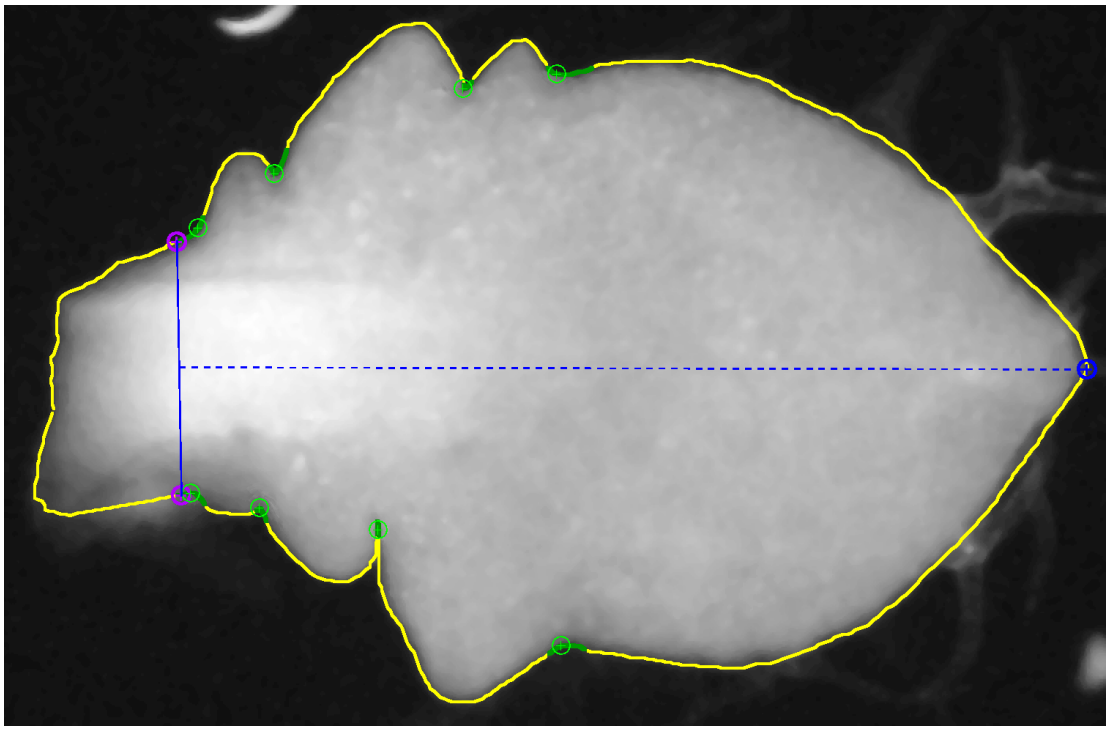

**Figure SM1. Segmentation of the leaf blade and determination of sinus landmarks.** The leaf contour is automatically segmented (contour in yellow). The blade contour is delimited by the manually positioned limits of the petiole (purple circles). The leaf apex (blue circle) is determined as the contour point at the greatest distance from the midpoint of the petiole limit (dashed segment). In each significant concave region (contour portions in green), a single tooth sinus is identified as the position with maximal negative curvature (green circles). Scale bar: 100µm.

*Teeth sinuses*

The identification of the teeth sinuses is based on the curvature of the contour. The local curvature is estimated at each position over the contour. The contour can then be decomposed into continuous convex or concave regions, the latter containing each a single sinus. To reduce the influence of insignificant contour oscillations, we only consider concave regions where the absolute curvature remains above a threshold value. In practice, the local curvature is computed from the outer angle formed by the position of interest and two neighboring contour points located within a given distance of the point of interest: the sharper the angle, the higher the curvature. In the MorphoLeaf application, the corresponding distance and threshold curvature are controlled by the "*Half Neighborhood*" and "*Maximal Negative Curvature*" parameters. Within each concave interval, the point with the maximal curvature (sharpest angle) is selected as a sinus (see Figure SM1).

*Teeth tips*

A single tooth tip is identified in each interval delimited by two consecutive sinuses (except between the two sinuses separated by the leaf apex in the case of pinnate leaves like in Arabidopsis). We developed two strategies to identify the tooth tip depending on the shape of the teeth:

- **Method 1.** For pointy teeth, the tip is identified as the point of maximal curvature, which is assessed using the same curvature measure used to identify the sinus positions but for inner angles. The *Half Neighborhood* parameter, which is expressed here as a fraction of the length of the leaf perimeter contained between two consecutive sinuses is the parameter controlling the calculation of the local curvature. Using such a parameter proportional to the size of the tooth instead of an absolute parameter enables a more accurate sinus tip identification when the size of the teeth is heterogeneous.

- **Method 2.** For rounded teeth, as for example those appearing at the margin of Arabidopsis primordia (Figure SM2A), the method described above was not accurate enough. We thus developed an alternative method based on local symmetry, starting from the observation that a rounded tooth can be seen (at least in the vicinity of its tip) to emerge from a shape that is symmetrical with respect to the tip. The recursive method we designed consists in identifying the optimal symmetry axis, which crosses the tooth contour at the tip location. The first candidate as a tip between two sinuses is the intersection between the tooth contour and the perpendicular bisector of the basis of the tooth (Figure SM2B). Besides, a reference sinus for the tooth of interest is identified as the sinus delimiting the largest half-tooth defined by the

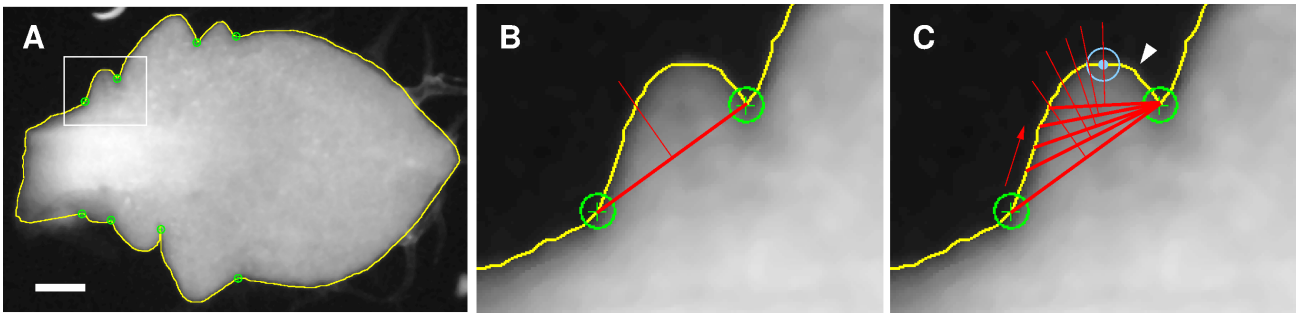


**Figure SM2. Determination of the tooth tip based on local symmetry.** A: a leaf contour (yellow curve) and teeth sinuses (green circles). B: zoom corresponding to the rectangle in A. The tooth basis (thick red segment) and the perpendicular bisector (thin red segment). C: search of the tooth tip which maximizes the local symmetry criterion (blue circle). White arrowhead: tip determined by the maximal curvature criterion. Scale bar: 100µm.

bisector (sinus on the right in Figure SM2B). Starting from the opposite sinus, successive points over the contour are considered, defining new bases (thick segments in Figure SM2C). At each step, the local symmetry is estimated by computing the ratio of the areas of the two regions delimited by the bisector and the basis. The contour position intersected by the axis with the maximal symmetry (e.g., a ratio close to 1) is chosen as the tooth tip (blue circle in Figure SM2C, to be compared with the solution given by the maximal curvature criterion, indicated by the arrow).

**Identification of the tooth hierarchy**

A primary tooth is defined as growing on the main leaf margin, while a secondary tooth is formed on a primary tooth. The objective is to retrieve this hierarchical structure by identifying secondary sinuses, *i.e.* sinuses that delimit secondary teeth only (as opposed to primary sinuses, at the basis of primary teeth). A proper hierarchy identification is crucial because the positioning of the sinuses is not sufficient to properly characterize the leaf serrations when secondary teeth occur on the contour (see Figure SM3). Note that a single sinus can delimit primary and secondary teeth at the same time.

To determine the tooth hierarchy, we designed two different approaches. Both are based on the observation that the shape defined by the primary sinuses is well aligned with the general leaf contour, i.e. a contour in which all teeth have been erased. On the contrary, secondary

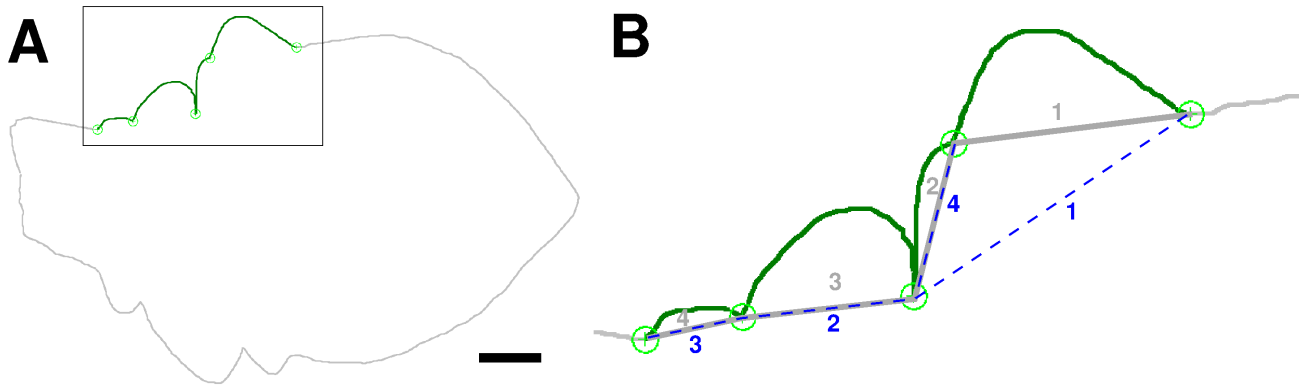


**Figure SM3. The sinuses identification is not sufficient to properly quantify leaf blade serrations.** A: contour of an Arabidopsis leaf, with the serrations of the upper half-leaf highlighted (green curve). Sinus positions are showed (green circles). B: zoom on the rectangle in A. Due to the presence of a secondary tooth, the position of the teeth is incorrect if we consider the sinuses sequentially. In gray: the numbers indicate four successive teeth that are incorrectly identified; their basal limits are indicated with continuous gray segments. In blue: the four teeth are correctly identified; their basal limits are indicated with blue dashed segments. Teeth 1, 2, and 3 are primary teeth while tooth 4 is a secondary tooth that is part of the primary tooth 1. Scale bar: 100µm.

sinuses are located further from this general contour. The first method (Method 1, described below) is efficient on a large variety of species, but fails on Arabidopsis because its leaves show a broad variety of tooth size along the blade during their development. We therefore developed a specific method to determine the hierarchy of developing teeth in Arabidopsis young leaves, based on a recursive process (Method 2, described below).

The two approaches described below apply to half-leaves (portion of the contour from the petiole to the leaf apex). The sinuses are ordered relatively to their successive positions on the contour (from the leaf apex to the petiole).

**Method 1.** The principle is to iteratively remove secondary sinuses until only primary sinuses remain on the contour. The method relies on the property that, contrary to secondary sinuses, primary sinuses are well positioned along the global leaf contour (*i.e.,* a contour without teeth). To quantify this, we use a curvature criterion: we compare the alignment of each sinus with its two neighbors and the local curvature at approximately the same position of the global leaf contour. These two measures should be similar at the position of primary sinuses, and significantly different for secondary sinuses. The shape of the global contour is approximated by drastically smoothing the initial contour (see Figure SM4AB). The smoothing is done using the strategy based on the elliptical Fourier descriptors introduced above, and the retained proportion of the power spectrum (degree of smoothing) is fixed as 50%. Initially, all sinuses are primary sinuses. The two bounding sinuses (first and last ones on the half-blade) are always primary. Sinus positions are projected onto the global smooth contour (see Figure SM4B, blue crosses). For each (non-bounding) sinus, we compute the angle formed with the two neighboring sinuses and the angle formed at the position of the projected sinus with two points in its vicinity on the global smooth contour. At each step, the candidate secondary sinus is the one for which the difference between these two angles is the highest (the pairs of compared angles for each candidate sinus are indicated by the same number in Figures SM4B and SM4C). If this difference is large enough (greater than a fixed threshold, the "*Stringency Factor*" in the MorphoLeaf application), the sinus is identified as secondary and removed from the set of sinuses (see the successive steps in Figure SM4C). Then, because a sinus is removed, the neighborhood relationship is changed for its two neighboring sinuses, thus the corresponding angles are recalculated accordingly. Otherwise, if the

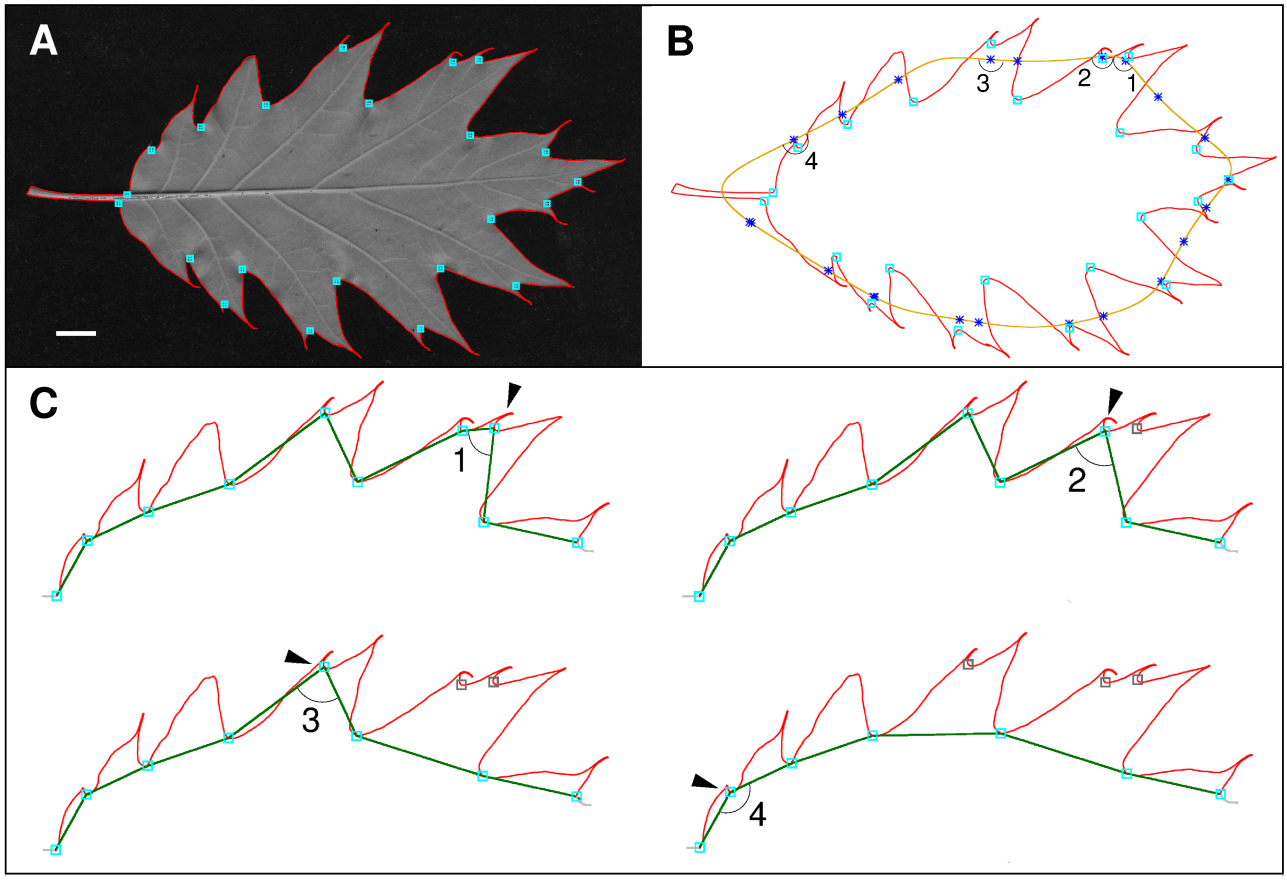


**Figure SM4. Hierarchy computation: the iterative method.** A: northern red oak (*Quercus rubra*) leaf image with the leaf contour (in red) and the teeth sinuses (light blue squares). B: Same segmentations as in A, with the projections of the sinuses (blue crosses) onto the general leaf shape (smooth contour, in orange). The numbered angles are related to the different steps of the method (see below). C: successive steps of the algorithm, applied to the sinuses of the upper half-leaf (red portion of the contour). Secondary sinuses are iteratively removed (gray squares). The green line connects the remaining sinuses. At each step, the candidate sinus (marked by an arrowhead) corresponds to the sinus that is the more distant from the general contour. Practically, the alignment of consecutive sinuses (angles in C) is compared to the curvature at the corresponding positions in the smooth contour (angles in B). At each step, the candidate is characterized by the greatest difference between the two angles (the pairs of angles corresponding to the successive candidates are indicated by a same number in Figs. B and C). The procedure stops when the angle difference is not significant anymore (step 4). Scale bar: 500µm.

difference is small, the procedure stops and the remaining sinuses are labeled as primary (see the final result in the last panel in Figure SM4C). In the MorphoLeaf application, the sole parameter of the method is the *Stringency Factor*.

**Method 2.** The idea behind this recursive method is to detect sinuses that are not well aligned with their two neighboring sinuses. The two extreme sinuses on either side of the contour at the current recursion are called bounding sinuses (initial bounding sinuses are pointed by arrows in Figure SM5A), and the portion of contour delimited by bounding sinuses is called a

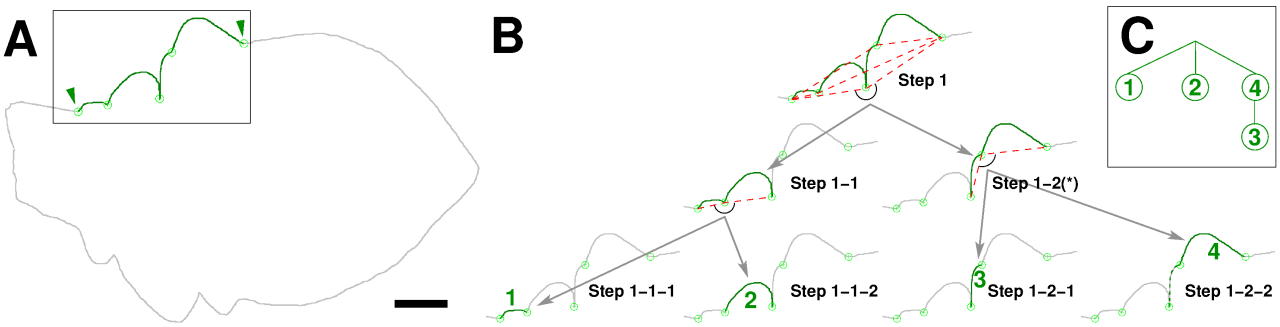


**Figure SM5. Hierarchy computation: the recursive algorithm of method 2.** A: a leaf contour (in gray) and the portion of the contour processed to build the hierarchy (in C), with the corresponding sinuses (green circles). Arrows: initial bounding sinuses. B: steps of the recursive procedure (the gray arrows illustrate the flow of the steps). The contour is recursively split into two sub-contours at the position of the sinus that maximizes the angle with bounding sinuses (red dash lines, maximal angle indicated by an arc). According to the angle value, a change in the hierarchy level is detected (star, step 1-2) or not (steps 1 and 1-1). The last row shows the final teeth, numbered in the order they were identified (tooth 3 is secondary). In step 1-2-2, the contour considered by the algorithm is indicated by the continuous green line, but the corresponding tooth (4) includes the green dashed line. C: corresponding hierarchy tree, with the same numbering as the one on the last row in B. Scale bar: 100µm.

lobe. The objective is to recursively build the hierarchy tree: the root corresponds to the base contour of the leaf (level 0) and the other nodes correspond each to a tooth, whose rank is determined by its level in the tree (a node of level 1 corresponds to a primary tooth, etc.). If the current lobe contains at least an inner sinus (i.e., distinct from the bounding sinuses; see, e.g., step 1 in Figure SM5B), the deepest sinus is determined as the sinus that forms the largest inner angle with the bounding sinuses (the deepest sinuses are indicated by arcs in Figure SM5B). This angle is used as a measure of alignment. The selected inner sinus splits the current lobe into two consecutive sub-lobes (in Figure SM5B, the split of the initial lobe yields the two sub-lobes highlighted in green in steps 1-1 and 1-2), and it becomes a bounding sinus in each of the two sub-lobes. If this sinus is sufficiently deep (if the angle is larger than a threshold, see below), no higher hierarchy is detected (steps 1 and 1-1 in Figure SM5B) and the same procedure is applied recursively on each of the two sub-lobes, with no change in the hierarchy (they are sister lobes). Alternatively, if the sinus is insufficiently deep (if the angle is smaller than the threshold, see below), the level of the sub-lobe with the smallest area is increased by 1, while the level of the other sub-lobe is unchanged (step 1-2 in Figure SM5B). In parallel, a new node is created at the current level in the tree that corresponds to the lobe with the largest area; this node is the mother of the sub-lobe, whose level is thus increased by 1. Next, the procedure is recursively repeated on each of the sub-lobes. The procedure stops when there is no more inner sinus, so that the current

lobe is a tooth (and a terminal node in the tree). The threshold angle determining whether the sinus is deep enough is chosen by the user in the MorphoLeaf application (*Limit angle* parameter).

**Validation of automatic landmark detection**

The correct identification of the teeth over the blade is crucial for the proper quantification of the blade shape. The teeth are defined by both the sinus positioning and their hierarchical organization. Therefore, we analyzed the performances of the MorphoLeaf application for the sinus detection and for the hierarchy identification by comparing automatic and manual results.

*Validation of the sinus detection*

To test the sinus detection procedure, two datasets were processed. Fifty images of Arabidopsis developing leaves and 10 of Northern red oak mature leaves, with blade contours and petiole limits previously segmented, were presented separately to 4 biologist experts. Using the *Free-D* software interface, each expert manually pointed the sinus positions over the leaf contours in the two datasets. In parallel, the automatic sinus segmentation of MorphoLeaf was applied to the data, with different values for the two parameters used in the module to determine sinuses positions: the Half Neighborhood and the angle defining the Maximal Negative Curvature.

For each image of the datasets, the first step consisted in automatically matching all segmented points (either defined by the experts or by MorphoLeaf) that correspond to the same biological landmark (see Figure SM6). Practically, points were sorted into different classes (showed with different colors in Figure SM6), so that each class corresponded to a single identified biological feature. Thus, a class contained at most one point from a given source (an expert or a given set of parameters). Each class that does not contain at least one point identified by an expert contains only false positives (false detection of a sinus; classes colored in white in Figure SM6). Conversely, each class that does not contain exactly the total number of sources contains at least one false negative (undetected sinus; for example, in Figure SM6, three pairs of parameters yielded false negatives in the class colored in light

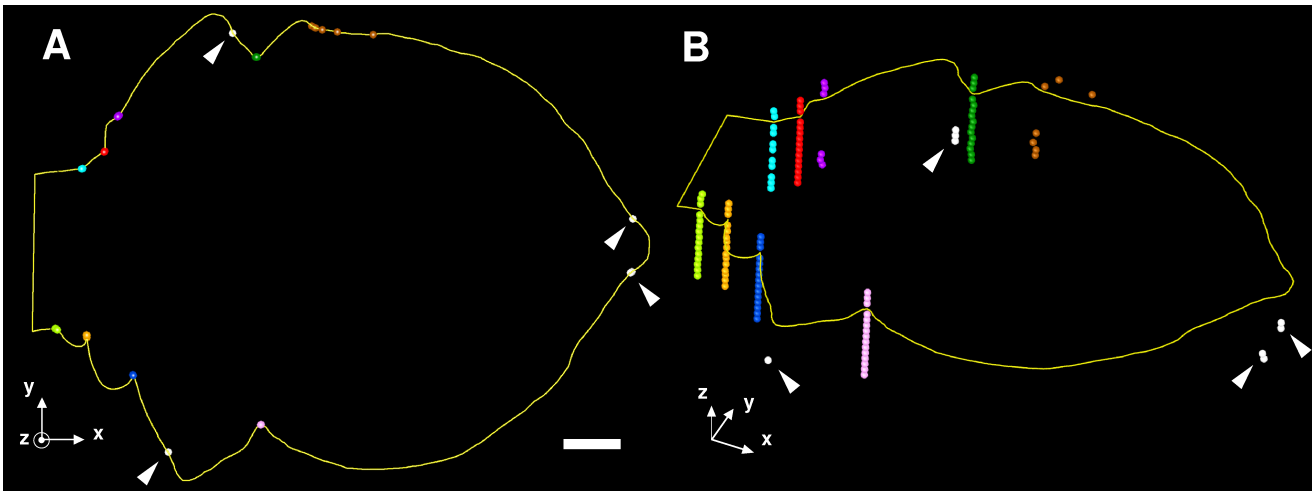


**Figure SM6. Determination of homologous landmarks classes from different sinus segmentations.** The positions of sinuses segmented over a blade contour (curve in yellow), either manually (here, by three biologist experts) or automatically (here, with 12 different pairs of parameters, same as in Figure SM7), are represented by colored dots. Points corresponding to a same biological landmark are put into the same sinus class and displayed with a specific color. Classes of false positives are all represented by white dots (arrowheads). A: standard 2D view of the contour and segmentations. B: tilted 3D view of A; for the sake of illustration, a different altitude (in the z-dimension) was assigned to each segmentation source, which is positive for each expert (points above the contour) and negative for the automatic method (points below the contour). The altitudes assigned to the different sets of parameters (from top to bottom) follows the same order than in Figure SM7. This representation was also used to visually inspect the accuracy of the sinus assignments to the different classes. Scale bar: 100µm.

blue). Once each detected point assigned to a sinus class, we considered three criteria to compare manual and automatic detections: accuracy, number of false positives and number of false negatives.

For all pairs of parameters, we measured the distances between the automatic detections and the sinuses identified by three out of the four experts (this set of three referent experts was thus considered as ground truth). Practically, within each landmark class (except false positive classes), the geodesic distance (distance along the contour) from each segmented point to the barycenter of the points from the set of referent experts was computed. For each set of parameters, these measures were averaged across all classes and all leaves in the data set and compared to the same measures computed for the remaining expert. Applied successively to all possible sets of three referent experts, this allowed us to compare the performances of each expert individually with the ones of the automatic method. The results are shown in Figures SM7A and SM8A. For the Arabidopsis dataset (Figure SM7A), the mean distances do not exceed 3µ*m*. This is remarkably low when compared to the leaf contour length in the data set (which ranges from 553µ*m* to 3930µ*m*, with an average length of

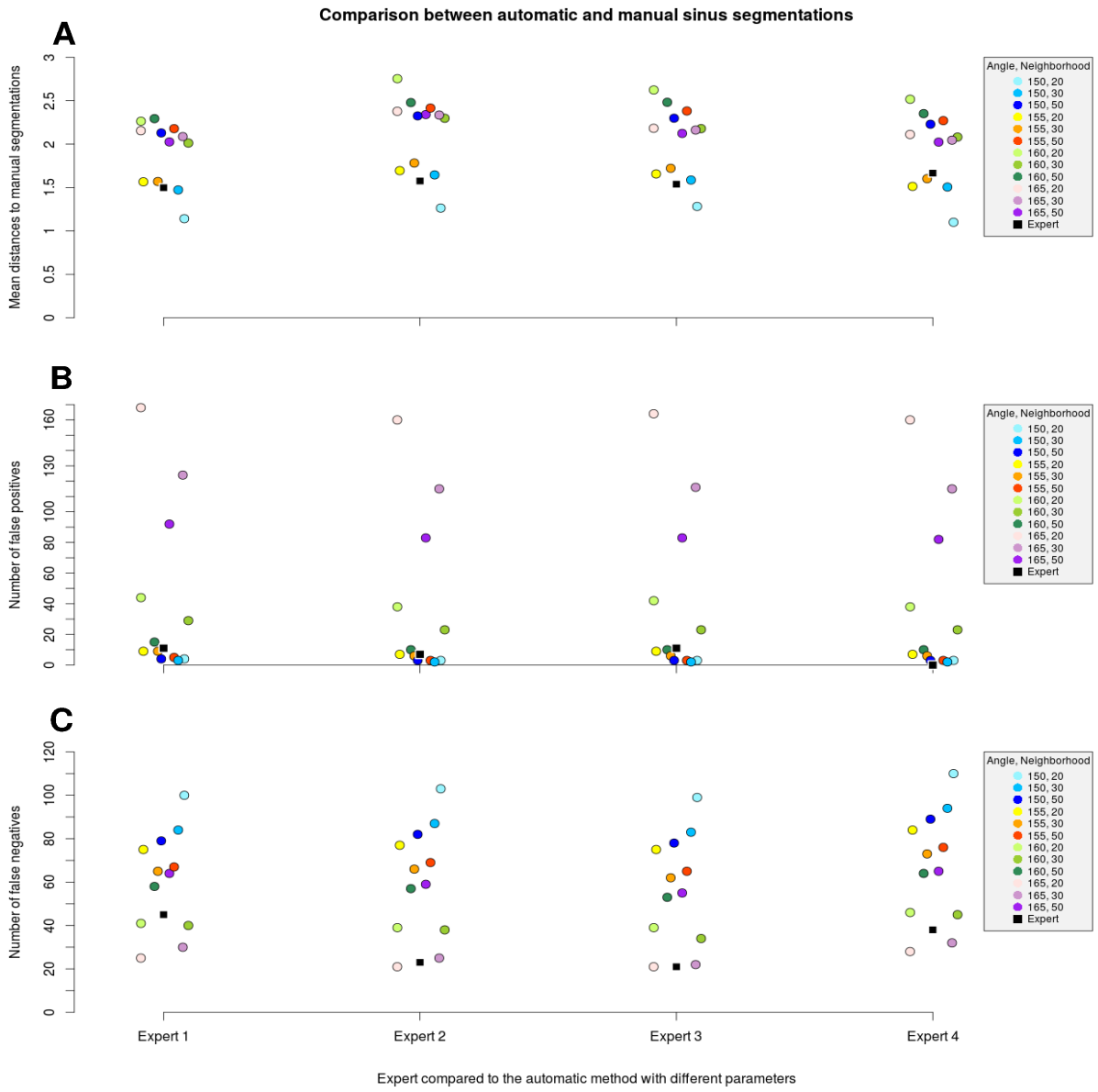


**Figure SM7. Comparison between manual and automatic sinus detections in Arabidopsis developing leaves.** A set of Arabidopsis leaf images was manually and independently analyzed by four biologist experts to extract the position of sinuses. In each of the four columns, the results obtained by one expert (black square) and by automatic detections with different parameters (colored dots) are compared to the detections performed by the set of the three reference experts. We considered three criteria: precision (distances in µm) (A), number of false positive (B) and of false negative (C) detections. See the text for details.

1738µ*m*). For all experts, the accuracy was close to the one reached by automatic detections, whatever the parameter values. This confirmed that the automatic method can be as accurate as expert detections. For the oak dataset (Figure SM8A), the contour lengths were longer (ranging from 68*cm* to 108*cm* for 15*cm*-long blades in average, with an average contour length of 90*cm*), but the mean distances always remained below 1*mm*, with three sets of

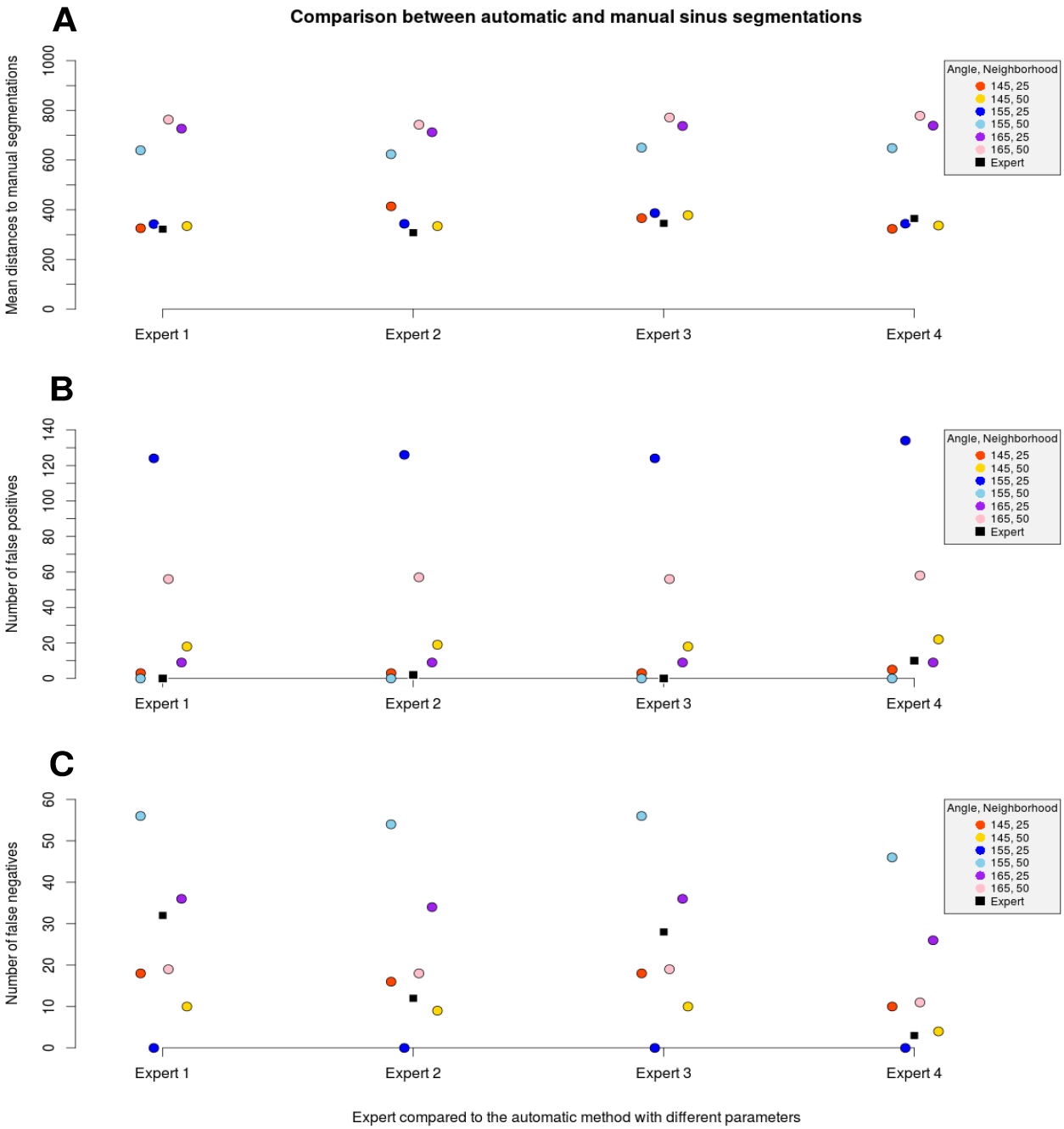


**Figure SM8. Comparison between manual and automatic sinus detections in Northern red oak mature leaves.** A set of oak leaf images was manually and independently analyzed by four biologist experts to extract the position of sinuses. In each of the four columns, the results obtained by one expert (black square) and by automatic detections with different parameters (colored dots) are compared to the detections performed by the set of the three reference experts. We considered three criteria: precision (distances in µm) (A), number of false positive (B) and of false negative (C) detections. See the text for details.

parameters that showed the same level of performance than the experts.

For Arabidopsis, a total number of 383, 405, 407 and 390 sinuses were detected over the 50

blade contours by Experts 1, 2, 3, and 4, respectively (in average, a number of 396 sinuses). The analysis of the number of false positive and of false negative detections (Figures S7BC) both showed a great variability according to the parameter values. Nevertheless, for each criterion, a set of parameters that provides satisfactory results that are comparable to those of the expert can be found. Concerning false positive detections, the 7 sets of tested parameters that provided the best results yielded less than 20 false positive points in total (i.e., 5% or less of the mean number of sinuses detected by the experts). These detections mainly occurred in the apical region of the blade, due to insignificant contour oscillations or to the two hollows on both sides of the leaf apex. The level of over-detection can be reduced by increasing the smoothing of the contours, but at the risk of eroding the real teeth. The number of false negative detections was slightly higher and was comprised between 20 and 80 for a large majority of parameters (between 5% and 20% of the mean number of sinuses detected by the experts). Experts 1, 2, 3, and 4 yielded 45, 23, 21 and 38 false detections, respectively. Hence, for both the experts and the automatic method, there was more false negatives than false positives. This is probably due to the specificity of the Arabidopsis dataset, which contains images of developing leaves in which the limits of emerging teeth are not pronounced and the sinus sometimes hardly visible.

For the oak dataset, a total number of 347, 367, 351 and 376 sinuses were detected over the 10 blade contours by Experts 1, 2, 3 and 4, respectively (in average, a number of 360 sinuses). If the numbers of false positive points were similar to the ones obtained for Arabidopsis, the level of false negative detections was significantly lower (Figures SM8BC), probably because the ambiguity in detecting teeth is lower in mature leaves than in developing ones. Four parameter sets generated 22 or less false positives points (6% or less of the mean total number of sinuses detected by the experts), while the majority of parameters (5 out of 6) yielded 36 or less false negative detections (10% or less of the mean total number of sinuses detected by the experts). As in the case of Arabidopsis, several sets of parameters provided a number of false positive or negative detections comparable to the results from the experts.

These results emphasize the compromise to be found between the amounts of false positives and of false negatives. In practice, we recommend the use of parameter values that minimize

the number of false negative detections at a price of a reasonable number of false positive points. In our opinion, it is indeed easier to visually detect and then remove false positive points with the tools provided by the Free-D software. It is generally possible to identify eligible parameter values by manually testing several parameters and by visually inspecting the corresponding results. In the case of our Arabidopsis dataset, an angle of 60 degrees and a neighborhood size of 30 pixels seems to be a good compromise that yields about 40 false detections and about 30 false positive points, which represent 10% and 7% of the true total number of sinuses, respectively. Concerning the oak dataset, an angle of 145 degrees and a neighborhood size of 25 or 50 pixels provided good overall results.

*Validation of the hierarchy procedure*

We quantified the performances of the two procedures available for the automatic tooth hierarchy identification. The method 1 was evaluated on a set of 10 northern red oak leaf images. The method 2 was evaluated on a set of 40 leaf images from Arabidopsis *mir164a-4* mutants, which present an increased level of leaf serrations (Nikovics et al., 2006). The two data sets were previously analyzed to extract the blade contours and the positions of petiole, apex and tooth tips and sinuses. Next, both data sets were presented separately to four experts. Each expert manually identified, among all the sinuses, the pairs of sinuses delimiting secondary teeth. For the two species, the hierarchy identification was identical for all experts, so that their results were considered as ground truth in the following analyses. Based on the method previously presented to match homologous segmented points (Figure SM6), we compared the manual identifications of secondary teeth to the ones obtained using the automatic methods. For this, we quantified the number of true and false positive (*TP* and *FP*) and negative (*TN* and *FN*) detections of secondary teeth, and computed the sensitivity (true positive rate, [*TP*/(*TP*+*FN*)]) and specificity (true negative rate, [*TN*/(*TN*+*FP*)]). Note that here, the TN detections correspond to primary teeth detections.

For northern red oak leaves, we applied the iterative method with four different values for the *Stringency Factor*. The results are presented in Table 1. All tested stringency values yielded satisfactory results with sensitivity and specificity both above 95%, with an optimal parameter value of 0.25.

| Northern red oak leaves (10 leaves) | | | | | | | | | | |
|---|---|---|---|---|---|---|---|---|---|---|
| **Stringency Factor** | **Total number of teeth** | **Total number of primary teeth** | **Total number of secondary teeth** | **Number of segmented secondary teeth** | **True positive (TP)** | **False positive (FP)** | **True negative (TN)** | **False negative (FN)** | **Sensitivity** | **Specificity** |
| **0.15** | 350 | 149 | 201 | 207 | 201 | 6 | 143 | 0 | **100%** | **96%** |
| **0.20** | | | | 203 | 201 | 2 | 147 | 0 | **100%** | **99%** |
| **0.25** | | | | 201 | 201 | 0 | 149 | 0 | **100%** | **100%** |
| **0.30** | | | | 194 | 194 | 0 | 149 | 7 | **97%** | **100%** |

**Table 1. Performance quantification of the iterative hierarchy method for secondary teeth detection.** The secondary teeth automatically segmented in northern red oak leaves by the iterative method, with four different parameters, were compared to the true segmentations defined by experts.

For Arabidopsis leaves, we applied the method with four different values for the *Limit Angle* parameter. The results are presented in Table 2. The evaluation of the recursive method showed that an angle around 45 degrees provides very satisfactory results, with a low number of false negative and positive detections, and both a sensitivity and a specificity above 90%.

| Arabidopsis thaliana leaves (40 leaves) | | | | | | | | | | |
|---|---|---|---|---|---|---|---|---|---|---|
| **Limit Angle parameter (in degrees)** | **Total number of teeth** | **Total number of primary teeth** | **Total number of secondary teeth** | **Number of segmented secondary teeth** | **True positive (TP)** | **False positive (FP)** | **True negative (TN)** | **False negative (FN)** | **Sensitivity** | **Specificity** |
| **35** | 345 | 317 | 28 | 12 | 12 | 0 | 317 | 16 | **43%** | **100%** |
| **40** | | | | 24 | 22 | 2 | 315 | 6 | **79%** | **99%** |
| **45** | | | | 35 | 26 | 9 | 308 | 2 | **93%** | **97%** |
| **50** | | | | 53 | 28 | 25 | 292 | 0 | **100%** | **92%** |

**Table 2. Performance quantification of the recursive hierarchy method for secondary teeth detection.** Secondary teeth automatically identified in Arabidopsis thaliana leaves were compared to the true segmentation defined by experts (third and fourth columns). Numbers of true and false positive (TP and FP) and negative (TN and FN) detections were evaluated, and the method sensitivity and specificity were computed for each parameter value (last two columns).

In conclusion, for both red oak and Arabidopsis leaves, the two methods for the automatic detection of secondary teeth showed very good performances.

## Estimation of growth trajectories

The blade shape evolution during growth can be estimated by averaging contours of different lengths during development. First, contours are sorted according to the blade length, so that

they are all distributed over a “length axis”. In parallel, all blade contours are reparametrized so that the landmarks which are biologically homologous across the data are put into correspondence. After this reparametrisation procedure, the contour portions comprised between the homologous landmarks in different leaves are composed of the same number of points. This ensures that the *p*-th point in a contour is homologous to the *p*-th points in all other contours. Thus, relevant mean shapes can be computed. Before the averaging, contours are aligned using a group-wise registration procedure (Maschino et al., 2006). Then, we proposed two approaches to estimate a growth trajectory based on the computation of mean blade contours. The first method is based on assigning leaves to different size classes and the second one on a moving (or sliding) average approach. For both methods, it should be stressed that a sufficiently dense sampling (with no gap) of the contours according to the blade length is critical for a proper estimation of the growth trajectory.

**Bin-based method.** The strategy consists in sorting the contours into different length classes (“bins”) on the length axis, and then in averaging all contours within each class. In the MorphoLeaf application, the user can specify the number of desired average contours (i.e., the number of classes). Then, the limits of the bins are computed so that all contain the same number of contours (total number of contours divided by the number of classes). Alternatively, the limits of the intervals can be manually specified, by loading in the application a file that contains the chosen limit values.

**Moving average method.** Instead of fixing intervals, this second approach (also called *Sliding average*) consists in using an adaptive kernel strategy (Parzen, 1962) for the contour averaging. At a given blade length $L$, all contours are used to compute the corresponding average. A weight is affected to each contour according to a Gaussian kernel function centered on $L$. Thus, only the contours whose lengths are close to $L$ significantly contribute to the averaging. The bandwidth parameter which controls the width of the kernel is computed locally and is equal to the distance from $L$ to the length of the $k$-th nearest contour on the length axis. This allows the bandwidth to adapt to the local density of contours on the length axis: the bandwidth is smaller when the number of contours with a length close to $L$ is high, and conversely. Besides, $k$ is a smoothing parameter: small $k$ values result in narrower bandwidths while high $k$ values lead to larger bandwidths (Figure SM9). The user can control


**Figure SM9. Effects of varying the neighbor rank in the sliding averaging on the mean shape.** Average Arabidopsis thaliana leaves of 504µm-long were reconstructed using the sliding average method from a set of 207 leaves of lengths ranging from 109µm to 2383µm. For each reconstructed average shape, the neighbor rank used and the resulting bandwidths are indicated.

the bandwidth by defining the *k* value (called *Neighbor Rank* in the MorphoLeaf application). It is possible to specify either the desired number of average contours (which are then equally distributed over the range of all lengths) or a set of specific lengths, by loading a file with the chosen values in the application.

A file with the local bandwidth at each mean shape is generated and can be used by the user to check the contribution of individual leaves to the mean shape.

## Bibliography

Kuhl, F. P. and Giardina, C. R. (1982). Elliptic Fourier features of a closed contour. *Computer Graphics and Image Processing*, 18, 236–258.

Maschino E., Maurin Y. and Andrey P. (2006). Joint registration and averaging of multiple 3D anatomical surface models. *Computer Vision and Image Understanding*, 101, 16–30.

Nikovics, K., Blein, T., Peaucelle, A., Ishida, T., Morin, H., Aida, M. and Laufs, P. (2006) The balance between the MIR164A and CUC2 genes controls leaf margin serration in Arabidopsis

*The Plant Cell* 18(11), 2929-45.

Parzen E. (1962). On estimation of a probability density function and mode. *The Annals of Mathematical Statistics*. 33(3), 1065–1076.

Vincent L. and Soille P. (1991). Watersheds in digital spaces: an efficient algorithm based on immersion simulations. In *IEEE Transactions on Pattern Analysis and Machine Intelligence*, 13(6), 583–598.